

Polymer Translocation: a Nonequilibrium Process

by

Sarah C. VOLLMER

*A Thesis Submitted in Partial Fulfillment
of the Requirements for the Degree of*

Master of Science

in

The Faculty of Science

Modelling and Computational Science

University of Ontario Institute of Technology

April 7, 2017


© Sarah C. Vollmer 2016

Declaration of Authorship

I, Sarah C. VOLLMER, declare that this thesis titled, "Polymer Translocation: a Nonequilibrium Process" and the work presented in it are my own. I confirm that:

- This work was done wholly or mainly while in candidature for a research degree at this University.
- Where any part of this thesis has previously been submitted for a degree or any other qualification at this University or any other institution, this has been clearly stated.
- Where I have consulted the published work of others, this is always clearly attributed.
- Where I have quoted from the work of others, the source is always given. With the exception of such quotations, this thesis is entirely my own work.
- I have acknowledged all main sources of help.
- Where the thesis is based on work done by myself jointly with others, I have made clear exactly what was done by others and what I have contributed myself.

Signed:



Date:

April 7 2017

"Paths are made by walking."

Franz Kafka

Abstract

Modelling and Computational Science

Master of Science

polymer translocation: a nonequilibrium process

by Sarah C. VOLLMER

3D Langevin dynamics simulations of the capture and translocation of polymers through a nanopore are conducted for several polymer lengths and two different Péclet values (that quantify the drift-diffusion balance of the system). By measuring the average conformation of the polymer and the average duration of each stage, simulations of the capture process reveal an elongated polymer approaching the nanopore and either remains elongated or becomes compressed just prior to translocation depending on the drift-diffusion balance. This is in direct contrast with the standard approach of simulating only the translocation process where the polymer is assumed to start translocation in an equilibrated state. The conformational differences directly impact scaling results of the translocation time by polymer length, where, even on a qualitative level, simulations that assume equilibration may yield incorrect results. The capture process is therefore an essential step for modelling and establishes the nonequilibrium nature of the translocation process.

Keywords: polymer, translocation, nanopore, nonequilibrium

Acknowledgments

Much appreciation is given to UOIT and everyone at Graduate Studies (in particular ATT). I would also like to extend a warm thank-you to all the Modelling and Computational Science staff and faculty (and members of the CNab Lab!) present from 2014-2016. Thank-you, VK: lab»tut!

My supervisor, Hendrick W. de Haan, deserves a big round of applause (or a bucket of craft beer) for seeing this through until the end- I am (one of) the first in what I am sure will be a very long line of successful (and funded!) graduate students to come! Finally, a thank-you to my committee members, LvV and IT, for overseeing the finishing touches.

Last but certainly not least- much love to my beautifully brilliant brother for his 'hilarious' edits and comments...and to CBJ for the introduction that started everything...

Contents

Declaration of Authorship	ii
Abstract	iv
Acknowledgments	v
Contents	vi
List of Figures	viii
List of Tables	ix
List of Abbreviations	x
List of Concepts	xi
1 INTRODUCTION	1
1.1 Polymer Translocation	1
1.1.1 Scaling Laws	2
1.2 Scope	3
1.3 Current Situation	4
1.4 New Approach	5
1.4.1 Result Highlights	6
2 BACKGROUND	7
2.1 Experimental Translocation	7
2.1.1 Biological Nanopores	7
2.1.2 Solid State Nanopores	7
2.2 Simulated Translocation	8
2.2.1 Polymer Chains	8
2.2.2 Molecular Dynamics	16
2.3 Tension Propagation	22
3 LITERATURE REVIEW	24
3.1 Introduction	24
3.1.1 Foundation	25

3.1.2	Experimental Work	28
3.1.3	Theoretical Work	33
3.1.4	Simulation Work	37
3.1.5	Tension Propagation and Capture Process	39
4	SIMULATION APPROACH	46
4.1	Translocation Conditions	46
4.1.1	Nanopore	46
4.1.2	External Field	47
4.1.3	Péclet Number	47
4.2	Simulation Protocols	50
4.2.1	Standard Protocol	50
4.2.2	Capture Protocol	51
4.3	Additional Considerations	56
4.3.1	Determination of R_{port}	56
4.3.2	Computational Details	60
5	RESULTS	61
5.1	Review of Results	61
5.1.1	Simulation Cases	61
5.1.2	Event Types	62
5.2	Polymer Configurations	63
5.2.1	Standard Protocol	63
5.2.2	Capture Protocol	66
5.3	Time Scales	77
5.3.1	Default Péclet	78
5.3.2	Tuned Péclet	80
5.3.3	Escape Process	82
5.4	Distribution of τ	84
5.4.1	Standard Protocol	86
5.4.2	Capture Protocol	86
5.5	Scaling Results	92
5.5.1	Trends: Standard Protocol	92
5.5.2	Trends: Capture Protocol	93
6	CONCLUSION	95
6.1	Summary	95
6.1.1	Evaluation	97
6.2	The Extended Model	99
6.2.1	Future adaptations	100
6.3	Final Remarks	101
	Bibliography	102

List of Figures

1.1	Polymer Translocation	2
2.1	Bonded Potentials	9
2.2	FENE Potential	10
2.3	Non-Bonded Potentials	11
2.4	WCA Potential	12
2.5	Radius of Gyration	14
2.6	Implicit vs Explicit Solvation	19
2.7	Tension Propagation	23
3.1	Tension Propagation - Tuned Péclet	41
3.2	Elliptical Cylindrical Coordinates	43
3.3	Oblate Spheroidal Coordinates	44
4.1	Nanopore	46
4.2	External Potential Field	48
4.3	Schematic of Capture Protocol Stages	52
4.4	R_{port} : Default P	58
4.5	R_{port} : Tuned P	59
5.1	Polymer Conformations: Standard Protocol	65
5.2	Polymer Conformations: Capture protocol	68
5.3	Detailed Polymer Conformations: Capture Protocol	72
5.4	Primary Contact Point of Polymer	75
5.5	Distribution of Threading Times	78
5.6	Monomer Index: Contact, First and Last Thread	81
5.7	Screenshot: Default P - typical	83
5.8	Screenshot: Default P - atypical	83
5.9	Screenshot: Tuned P	84
5.10	Distribution of Translocation Times	87
5.11	Scatter Plot: N50	89
5.12	Scatter Plot: N100	90
5.13	Scatter Plot: N200	91
5.14	Scaling Results: τ vs N	93

List of Tables

5.1	Counts of Capture Protocol Event Outcomes	63
6.1	Average Durations of Capture Protocol Phases	97

List of Abbreviations

DNA	DeoxyriboNucleic Acid
dsDNA	double stranded DNA
ssDNA	single stranded DNA
N	Number of monomers (effective polymer length)
P	Péclet number
TP	Tension Propagation
R_g	Radius of Gyration
$R_{g_{eq}}$	Radius of Gyration (Equilibrium)
$R_{g_{\parallel}}$	Radius of Gyration (Parallel)
$R_{g_{\perp}}$	Radius of Gyration (Perpendicular)
SD	Standard protocol under Default Péclet conditions
ST	Standard protocol under Tuned Péclet conditions
CD	Capture protocol under Default Péclet conditions
CT	Capture protocol under Tuned Péclet conditions
C	Contact event
FT	First Thread event
LT	Last Thread event
T	Translocation event

List of Concepts

monomer	discrete repeatable unit of a polymer
polymer	a chain of linked monomers
radius of gyration	2^{nd} moment of mass distribution and the characteristic size of the polymer
nanopore (pore)	a small hole in a membrane
translocation	the passage of a polymer across a membrane
<i>cis</i> side	the side of a pore where polymer translocation begins
<i>trans</i> side	the side of a pore where polymer translocation ends
biased (forced) translocation	translocation that occurs with an applied force
unbiased translocation	translocation that occurs without an applied force
electrophoresis	charged polymers moving in a gel or liquid due to an electric field
Péclet number	value used to indicate the drift-diffusion balance
default P	typical Péclet number used in current literature
tuned P	an alternative Péclet number tuned to experiment
standard protocol	simulation methodology focusing only on translocation
capture protocol	translocation simulation including capture

*To my family..
you created my body, nurtured my mind, and
protected my soul - GDSDVOL you are why I can...*

*.:)PNP(:.
1 12 101 12 1
13 101 13
(113 || 127) && (2027 -> 11)*

*RIP Peter, Hildegard, Margery, Heinz - four of the best
grandparents anyone could have ever wished for.
This is especially for you. <3.*

Chapter 1

INTRODUCTION

1.1 Polymer Translocation

The study of polymers is a subset of soft matter physics and biological research. Within polymer science lays an important process known as polymer translocation that has much biophysical significance and can be found in DNA systems. Though reference to DNA is the most notable example, polymer translocation implies the passage of any molecular chain through a membrane via a nanopore. The nanopores may be synthetic, and the chains may be stiff and rod-like or they may have any degree of flexibility, able to fold in on themselves many times over. What remains consistent is the repetition of smaller molecular sub-units joined together to form the bulk of the chain. Fig. 1.1 illustrates a typical polymer translocation event.

Apart from purely academic efforts, advances in engineering and medical research have opened the path towards genetic mapping through DNA sequencing, and the ability to filter polymers by their constituents, or even by their length and size, paves the way for customized applications. Currently, computational methods have increasingly made use of high performance computing networks with access to computational power able to run many complex

calculations with high efficiency. These systems have made it possible to design simulation models to understand these fundamental biological processes.

Polymer translocation is one such process that, to properly quantify the dynamics at play, has drawn attention from both physical and computational inquiry. A particularly cross-disciplinary area of research, progress is made through, among others, the following research endeavours: Theoretical models of transport dynamics; Experimental observation of biological and chemical attributes of different polymers, membranes and solvents; Nanoengineering of synthetic nanopores; Stochastic computational models that produce relevant physical pictures.

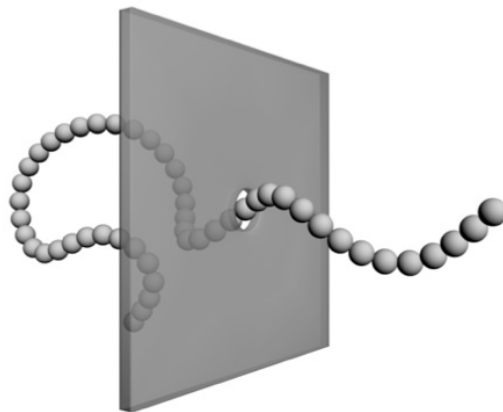


FIGURE 1.1: A schematic of polymer translocation[36].

1.1.1 Scaling Laws

Uncovering a fundamental functional relationship between two physical parameters permits a quantitative understanding that can potentially be applied over many orders of magnitude. Arguably, scaling laws provide one of the most efficient means of comparing quantities, particularly so in biology, where systems are highly complex. Thus, in the domain of polymer physics, and in

particular studies of translocation, a means of describing polymer behaviour that scales with length is desirable. This is largely due in part to the many variations of polymer chains that exist, and the common process of translocation that they can all naturally (or synthetically) be induced to undergo.

The body of this work is concerned with assessing the qualitative picture assumed in current translocation simulations and the quantitative changes that arise such as the scaling of translocation time to a polymer's length. To date, most standard simulation models of translocation fall short of reproducing the scaling properties observed in experiment. With the ability to run a large number of events, simulations are able to provide relevant contributions to research questions so long as the design is physically correct. By improving upon simulations of the translocation process they will necessarily become more relevant and beneficial to the field of polymer science in general.

1.2 Scope

This thesis focuses on the use of computational molecular dynamic methods to simulate the passage of a polymer through a nanopore. Specifically, Langevin dynamics are used where solvent interactions are implicitly included in the equation of motion. Polymer motion is characterized by random thermal kinetic energy and through force effects of an externally applied potential difference related to the geometry of the system. A correct picture of the drift-diffusion balance is important for both understanding and manipulating translocation dynamics, particularly in device fabrication such as DNA sequencers.

This work focuses on comparing and contrasting the existing standard simulation design for polymer translocation to a newly devised approach. This

new model simulates the capture process in addition to translocation, and uses values for the Péclet number to describe the drift-diffusion balance. Methods of quantification include describing the polymer's conformation through its radius of gyration, timescales of the simulation stages, and scaling relationships across polymer length.

Important stages of the capture process, such as the initial equilibration state, nanopore contact, and threading events, are used to document the path of a polymer until it has successfully translocated. By adapting the standard model to include the capture process of a polymer by a nanopore it was possible to comment on the universality of translocation dynamics arising from a variety of initial polymer configurations. The objective of this work is to therefore determine if the capture process impacts translocation. This may also offer insight to bring experiment and simulation into closer agreement.

1.3 Current Situation

At present, most computational models of polymer translocation adopt a similar simulation design. These simulation approaches typically begin by fixing at least one monomer within the nanopore prior to translocation. The polymer is left to equilibrate in this state and is then released and the translocation dynamics are tracked. Field effects are contained within the nanopore and only monomers passing through the nanopore feel the force and are driven through. All other monomers are only exposed to diffusive dynamics regardless of which side of the nanopore they are found on. Contention in literature arises from scaling exponent inconsistencies which may or may not match experiment.

1.4 New Approach

Under experimental as well as natural biological conditions, defining the applied field as existing solely inside the nanopore is unrealistic. Additionally, it is also unnatural to equilibrate and begin translocation of the polymer while it is held in place within the nanopore. This equilibrated conformation at the start of translocation is questionable, particularly as experimental observations indicate that there are a variety of parameters which affect the polymer as it moves towards a nanopore prior to translocation. Thus, a new methodology was developed to address these conditions in a coarse-grained simulation by modelling the full capture process of a polymer by a nanopore. The objective was to then test whether this more natural setup, which includes capture, would make a difference.

The capture method has several improvements over the standard simulation methodologies, but primarily it consists of mapping the full field profile without prematurely truncating it outside the nanopore and equilibrating the polymer away from the nanopore. By equilibrating the polymer away from the nanopore, both the diffusion of the polymer towards the nanopore as well as the effect of the driving force from the applied field could be measured as the polymer completes the capture-translocation process. As changes in the drift-diffusion balance may affect the movement of the polymer, it was thought that this may be reflected in the conformation of the polymer, thus affecting the translocation time and scaling relationships.

1.4.1 Result Highlights

A brief survey of the results indicate that the capture methodology does in fact give a new qualitative picture of the translocation process and is successful in identifying how a polymer's configuration immediately prior to translocation will alter the dynamics. Quantitatively, this could bring simulation results into closer agreement with experimental results. By mapping the entire capture process and by comparing changes in the drift-diffusion balance of the system, the obtained scaling results indicate that the standard model is qualitatively insufficient and that modelling the capture process may in fact be necessary for accurately describing the translocation process.

Chapter 2

BACKGROUND

2.1 Experimental Translocation

Before discussing the details of polymer translocation simulations, a brief description of the nanopores used in experimental translocation studies is presented.

2.1.1 Biological Nanopores

Biological nanopores are typically created in cell membranes via a pore-forming protein. In current research, α - *Hemolysin* protein is often used as the pores formed via this protein are naturally found in cell membranes. The pores are on the order of $1nm$ in diameter at the narrowest point and facilitate the transportation of ions and molecules in and out of the cell [6]. As ssDNA is on a similar scale, α - *Hemolysin* nanopores provide a desirable model for polymer translocation and genetic applications.

2.1.2 Solid State Nanopores

To create easily reproducible nanopores in a cost effective and efficient way, nanopore research has turned to manufacturing solid state nanopores from

synthetic materials. The use of these materials allows customization and exploration of the effects of different material compositions and is advantageous to mass production for a variety of applications. Often SiN and SiO_2 materials form the membrane substrates and are $30nm$ thick. The nanopore diameter can be controlled as an electron beam is used to drill the hole. Among other methods of fabrication, the use of high electric fields, which permit a controlled dielectric breakdown of the membrane, have recently been developed and provide a cost-effective alternative to nanopore fabrication suitable for mass-production [5, 51, 11].

2.2 Simulated Translocation

Coarse-grained simulations were used to model freely-jointed polymer chains and their complete translocation through a nanopore. The duration of key phases in the translocation process as well as the physical configuration of the polymer at each phase were recorded. Two different simulation protocols were used; one that focused solely on translocation and another that included the capture process leading up to and including translocation.

2.2.1 Polymer Chains

Coarse-grained Simulations

The goal of coarse-grained simulations is to reduce the number of degrees of freedom and interactions that are modelled. This approach allows complex polymers, such as dsDNA, to be simulated by reducing (bonded) molecules in the chain into individual 'pseudo-atoms'. In polymer science a pseudo-atom

is commonly referred to as a 'monomer'. The polymers simulated here are therefore comprised of these identical monomers bonded together in a chain.

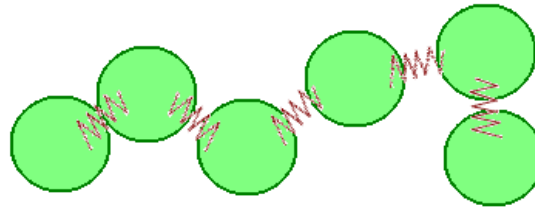


FIGURE 2.1: Similar to springs connecting two beads, bonded potentials represent the connection between adjacent monomers.

With the goal of developing a more comprehensive physical picture of the dynamics of polymer translocation, this simplification is more than adequate. By stripping away the more detailed atomic interactions pertaining to any one particular polymer, the fundamental physical interactions common to the translocation *process* may be explored. Once a reliable model is achieved through coarse-graining, future simulations tailored to the peculiarity of a specific polymer may progress, confident that any insight obtained is not an artifact of a qualitatively incorrect model of this transport process. Thus, by focusing on the methodology of the protocol, an improved computational tool is accessible to a much larger research body.

As scaling laws are a common means of comparing polymer physics results, the coarse-grained models used here simulate polymers with lengths $N = 50$, 100, and 200 where N is the number of monomers in the freely-jointed polymer chain.

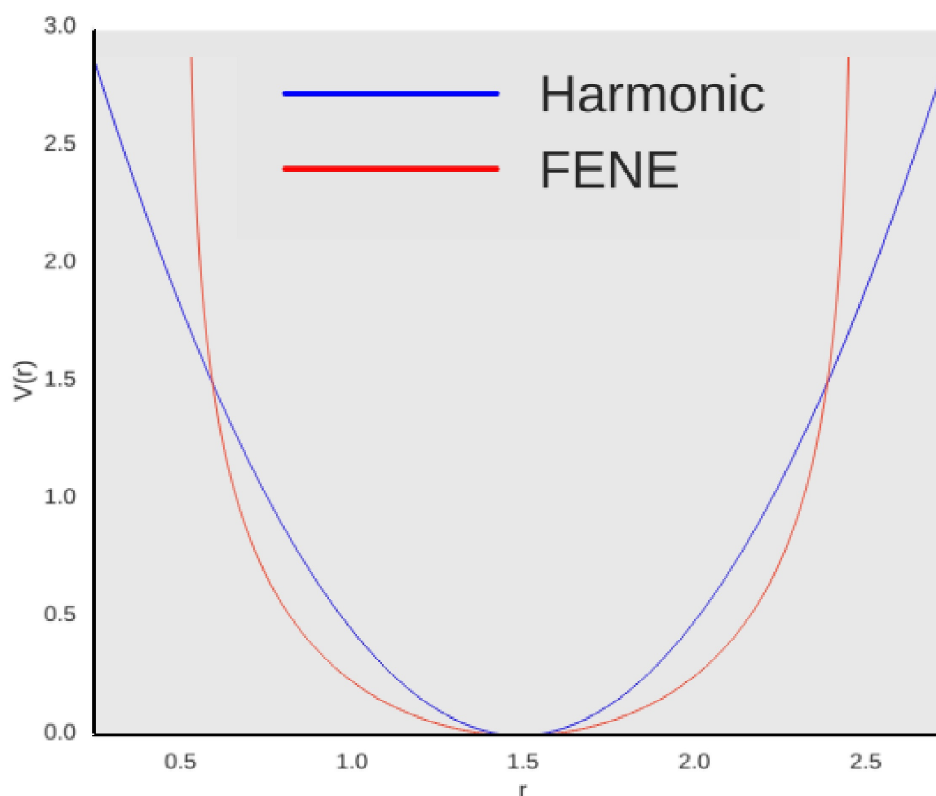


FIGURE 2.2: A comparison of the standard harmonic potential and the FENE potential used in computational models to simulate the push and pull of bonded monomers along a chain.

Bonded Potential

FENE Potential The **F**initely **E**xtensible **N**on-linear **E**lastic, or FENE, potential describes how adjacent monomers are bonded to one another along the polymer chain. Conceptually, the model likens the polymer chain to a series of beads attached to one another by a spring. Here, the spring is simulated by adapting a standard harmonic potential such that the potential's divergent behaviour will constrain maximum and minimum spring extension. Thus the

FENE potential provides clear boundaries to control the extension of the simulated bonds. Fig. 2.2 indicates the similarity of the FENE and harmonic potentials near $r = r_o$.

The FENE potential is quantified by:

$$V_{\text{FENE}}(r) = -\frac{1}{2}kr_0^2 \ln\left(1 - \frac{r^2}{r_0^2}\right). \quad (2.1)$$

All simulations here follow the model of Kremer and Grest where standard values r_0 and k in Eq. 2.1 were set as follows: $r_0 = 1.5\sigma$ and $k = \frac{30\epsilon}{\sigma^2}$ [31].

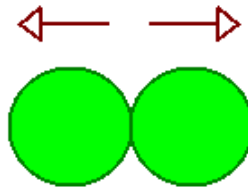


FIGURE 2.3: Non-bonded potentials provide repulsion.

Non-Bonded Potential

Excluded Volume A freely-jointed polymer chain is a linear collection of monomers connected to one another. These connections represent the bonds attracting any two adjacent monomers. As the computational model is simulating a real physical process, excluded volume effects are taken into consideration.

The excluded volume describes a small region of space that extends outward from a monomer preventing other monomers along the chain from occupying the same physical space in the same timestep. Likewise, this volume effect also prevents the polymer from unrealistically passing into or through the simulated membrane instead of threading the nanopore.

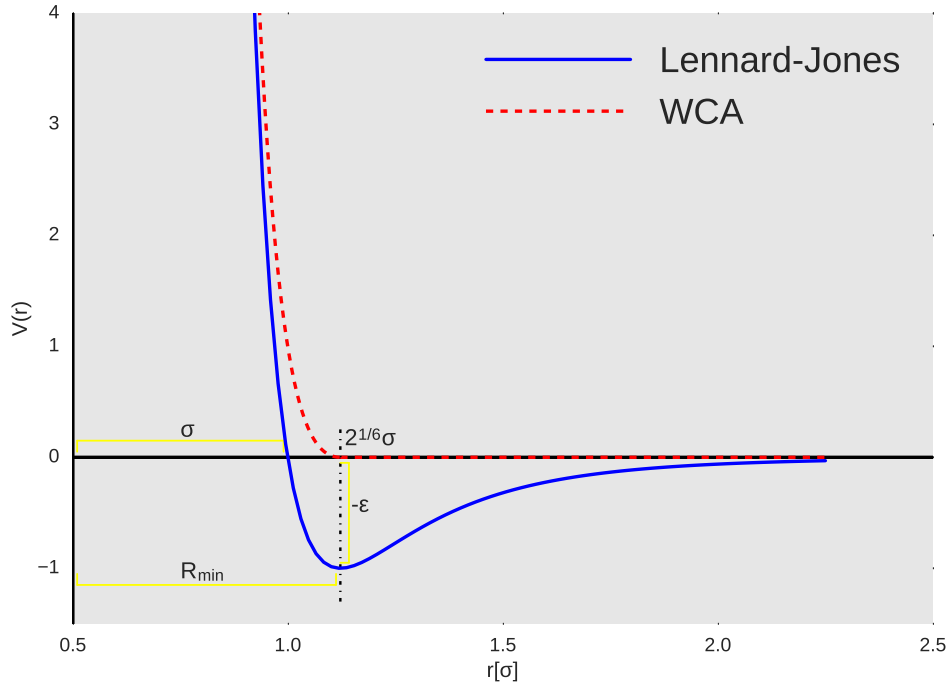


FIGURE 2.4: The standard Lennard-Jones Potential used to model long-range atomic interactions. When shifted and truncated, the LJ Potential is referred to as the WCA Potential and is commonly used for computational efficiency.

WCA Potential In molecular dynamics calculations many of the interactions are two-bodied repulsion interactions between monomers. Modelled as an intermolecular pair-potential, the standard methodology to handle these interactions is with a shifted and truncated Lennard-Jones potential, known as the **Weeks Chandler Andersen**, or **WCA**, potential [94]. This adjusted potential also includes the interaction of the monomers with the membrane and is given by:

$$V_{WCA}(r) = \begin{cases} 4\epsilon \left[\left(\frac{\sigma}{r}\right)^{12} - \left(\frac{\sigma}{r}\right)^6 \right] + \epsilon & \text{for } r < r_c \\ 0 & \text{for } r \geq r_c \end{cases} \quad (2.2)$$

where ϵ is the depth of the potential well; σ describes the effective size of the monomers; r is the distance between particles; and $r_c = 2^{1/6}\sigma$ is the cutoff distance and corresponds to where the Lenard-Jones potential is at a minimum.

Fig. 2.4 compares the standard Lenard-Jones potential to the shifted and truncated WCA form. Shifting the LJ potential upwards effectively eliminates the potential well that acts as an attractive force; truncating the shifted potential at the $r_c = 2^{1/6}\sigma$ cutoff sufficiently models the repulsion interactions. Although the total WCA potential is repulsive, it is still comprised of repulsive $((\frac{\sigma}{r})^{12})$ and attractive $((\frac{\sigma}{r})^6)$ components. Here at r_c , the LJ potential is at its minimum, which is then translated upwards to $V(r_c) = 0$. This allows the potential to decrease down to 0 with no discontinuity in the profile from integrating the conservative force.

Radius of Gyration

The radius of gyration, R_g , of a polymer can be described as the mean square distance between each monomer and the center of mass and is defined by Eq. 2.3 and Eq. 2.4. The polymer chain shown in Fig. 2.5 is in a typical relaxed configuration. Here r_{CoM} is the center of mass for the entire polymer chain and r_i represents any monomer along the chain. The enclosed circle indicates the average distance the monomers lie from the center of mass. Although Fig. 2.5 is a two dimensional image, the same principles apply when extending to three dimensions.

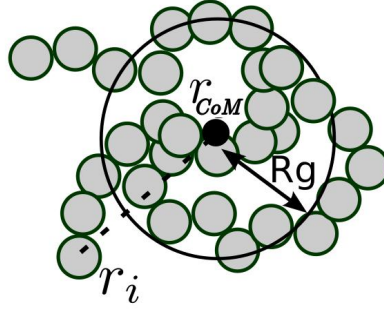


FIGURE 2.5: The radius of gyration, R_g , of a polymer is found by averaging the mean square distance between each monomer, r_i and the center of mass, r_{CoM} [91].

$$r_{CoM} = \frac{1}{N+1} \sum_{i=0}^N r_i \quad (2.3)$$

$$R_g^2 = \frac{1}{N+1} \sum_{i=0}^N \langle (r_i - r_{CoM})^2 \rangle \quad (2.4)$$

Due to the cylindrical symmetry of the system, two orientations of R_g are defined- the perpendicular and parallel orientations. R_g along the axis of the nanopore is defined as $R_{g\parallel}$, or R_g parallel. R_g perpendicular, $R_{g\perp}$, is described as the average R_g of both directions corresponding to the plane of the membrane (which is orthogonal to the axis of the nanopore). Thus a quantifiable three dimensional picture of the polymer's configuration and path during translocation can be recorded.

Relaxation Time

The relaxation time, τ_{Rx} , of a polymer is a measure of how long it takes a polymer chain to have its current conformation be uncorrelated to a prior 'initial' conformation. The conformational changes arise after the polymer has been

disturbed in some way, where, over time, its shape is altered. The disturbance could, for example, be the result of mechanical or electrical elongation or compression of the polymer, or even a result of continuous solvent interactions. The relaxation time is related to a polymer's diffusion coefficient, D , its radius of gyration, R_g , and also to its length, N . Here the diffusion coefficient describes the motion of the polymer's center of mass.

Starting with the definition of Brownian motion:

$$\langle \Delta r^2 \rangle = 6Dt \quad (2.5)$$

the following parallels are drawn: $\langle \Delta r^2 \rangle \Leftrightarrow R_g^2$ and $t \Leftrightarrow \tau_{Rx}$.

Thus, the relaxation time, τ_{Rx} , can be described by:

$$\tau_{Rx} \sim \frac{R_g^2}{D} \quad (2.6)$$

where R_g^2 represents the root mean squared (end to end) distance of the polymer chain i.e., the distance the polymer travels to relax is related to its own length and is given by the radius of gyration, R_g . When divided by the diffusion coefficient for the polymer in question, this equation describes how long it takes for a polymer to diffuse across itself- where it will have undergone enough changes in its conformation to be unrelated in shape to an initial configuration.

Since a polymer will experience drag in a viscous fluid as it moves, the length of a polymer will directly impact this mobility. Diffusion can then be described through as inverse relationship to a polymer's length $D \sim N^{-1}$, where the relaxation time is also given by:

$$\tau_{Rx} \sim \frac{R_g^2}{D} \sim \frac{R_g^2}{\frac{1}{N}} \sim R_g^2 N \quad (2.7)$$

Under these conditions a polymer is said to be experiencing **Rouse dynamics** and describes an ideal chain. However, the Rouse model overestimates the decrease in diffusion found in experiment, and a new model incorporating hydrodynamic interactions was developed. The diffusion here is referred to as **Zimm dynamics** and is given by $D \sim N^{-\nu}$, where ν is the Flory exponent, and is consistent with experiment for dilute polymer solutions with $\nu = 3/5$. Here correlated motion arising from the hydrodynamic polymer-solvent interactions permits faster relaxation times. Therefore, taking $R_g \sim N^\nu$:

$$\tau_{Rx} \sim (N^\nu)^2 N = N^{2\nu+1} = (N^{3/5})^2 N = N^{2.2} \quad (2.8)$$

An exponent, commonly referred to in literature as $\alpha = 1 + 2\nu$, is extracted from Eq. 2.8 and provides a way to quantify scaling results found for ν in experiment.

2.2.2 Molecular Dynamics

Molecular dynamics are computational methods in which the dynamics of a system (molecular, biological, material) can be described. Through the integration of Newton's equation of motion, different configurations of the system are generated by obtaining information regarding the positions and velocities of the particles in the system. In this way, macroscopic properties may be investigated through these microscopic simulations via the application of statistical mechanics. For equilibrium, the distribution of the system follows the Boltzmann distribution. As the system evolves over time, many possible states can be explored where it is often possible to comment on and interpret macroscopic behaviour.

Equation of Motion

The physical conditions for the simulated environment are built from Newton's second law, $\vec{F} = m\vec{a}$. If the force acting on an entity can be known, (e.g., an entity such as an atom in real life or a monomer in a simulation), then it is possible to determine the acceleration of this object, as the mass is typically known.

The force derived from Newton:

$$\vec{F} = m\vec{a} \quad (2.9)$$

For conservative forces, \vec{F} can also describe a potential (V) gradient ($\vec{\nabla}$):

$$\vec{F} = -\vec{\nabla}V \quad (2.10)$$

By equating Eq. 2.9 and Eq. 2.10, a trajectory can be found through the following differential equation:

$$\frac{dV}{dr} = -m \frac{d^2\vec{r}}{dt^2} \quad (2.11)$$

However, an analytical solution is not readily obtainable and numerical integration is therefore used to solve the differential. Once solved, a trajectory describing the positions, velocities, and accelerations of all bodies of interest as they move over time can be determined.

Integration A common method of integration to obtain the state of the system is through a *Velocity Verlet* algorithm. As forces are provided to the simulated system it is possible to extract, or define, the acceleration via $\vec{a}(t) = \vec{F}(t)/m$. The initial step for describing the motion of the particles in a system

is to provide starting accelerations $\vec{a}(t)$, velocities $\vec{v}(t)$, and positions $\vec{x}(t)$ for all particles in motion.

The position of a particle at $t = t + \Delta t$ is therefore given by:

$$x(t + \Delta t) = x(t) + v(t)\Delta t + \frac{1}{2}a(t)\Delta t^2 \quad (2.12)$$

Once the position is known, the velocity halfway through the time step Δt can be found:

$$v(t + \frac{1}{2}\Delta t) = v(t) + \frac{1}{2}a(t)\Delta t \quad (2.13)$$

The new acceleration, $a(t + \Delta t)$ is derived again from $\vec{a} = \vec{F}/m$ using $x(t + \Delta t)$, and finally, the full velocity can be computed via:

$$v(t + \Delta t) = v(t + \frac{1}{2}\Delta t) + \frac{1}{2}a(t + \Delta t)\Delta t \quad (2.14)$$

These integration steps are repeated for each particle at every time step.

Langevin Dynamics

Langevin dynamics is a method of mathematically modelling the solvent dynamics of a given system. Through the use of stochastic differential equations, Langevin dynamics allows for a solvent to be implicitly included in the equation of motion; the effects arising from each solvent monomer are combined into average forces which can be calculated over the entire simulation space at each time step. This approach alleviates much of the computational overhead by removing a large portion of the interactions between polymer and solvent.

Fig. 2.6 illustrates that with explicit solvation, the solvent is modelled as individual particles where each solvent interaction must be calculated for every

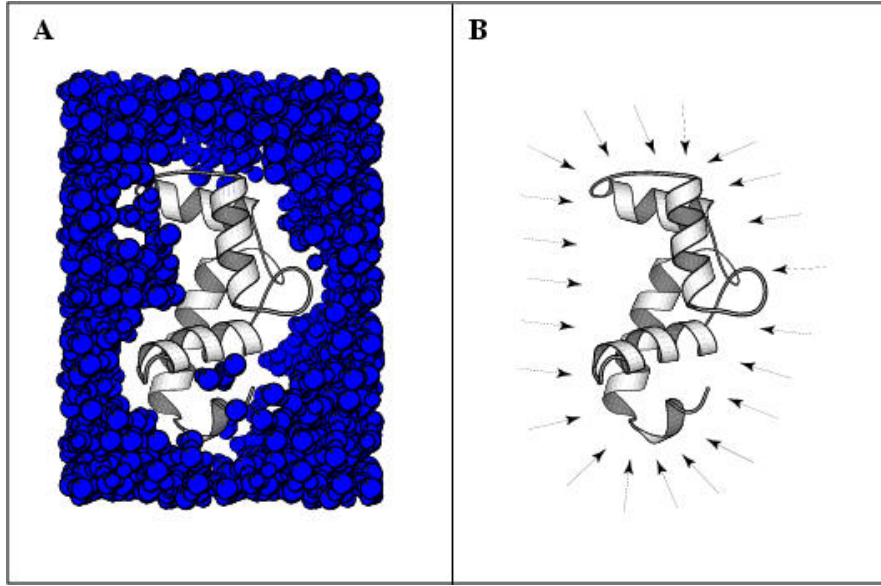


FIGURE 2.6: Explicit (A) v Implicit (B) solvation methods for computational models. In explicit solvation, interactions between all solvent molecules are calculated individually. In implicit solvation, the solvent is modelled as an average field. [48]

monomer. For implicit solvation, there is a *massive* drop in individual calculations performed by modelling the solvent as a force. Minimizing the computational cost per time step is an important design criterion in simulation modelling. Here the solvent is included implicitly in the Langevin Equation through the addition of a random force term and a damping term:

$$m\vec{a} = -\nabla U(\vec{x}) - \gamma\vec{v} + \sqrt{2\gamma k_B T}\vec{R}(t) + \vec{F}_{ext} \quad (2.15)$$

where γ is the friction coefficient (γ/m represents the collision frequency), $-\nabla U(\vec{x})$ is the sum of the conservative forces and represents the external field applied to the system. \vec{F}_{ext} represents any additional external forces on the system, and

$\vec{R}(t)$ is a random term where:

$$\langle \vec{R}(t) \rangle = 0 \quad (2.16)$$

$$\langle \vec{R}(0) \cdot \vec{R}(t) \rangle = \delta_{i,j} \delta(t) \quad (2.17)$$

with i, j corresponding to the Cartesian coordinates and $\delta(t)$ being the Dirac delta function.

In Eq. 2.15 the random term, $\vec{R}(t)$, must satisfy a number of conditions to reproduce the random thermal motion of the solvent interactions on the polymer. First, the mean of the applied force must be zero for it to be stationary and second, the random force must be considered uncorrelated in time, similar to white noise. Both the viscous drag and the random force are not independent of each other as they are both due to the solvent interactions.

Diffusion

Diffusion is a process by which a particle moves as a result of energy from random, thermal motion. The fluctuation-dissipation theorem states that for processes that dissipate energy via heat there is a corresponding reverse process described by thermal fluctuations. γ , the frictional force on a small spherical particle of radius R and mass m , relates this dissipation to corresponding Brownian motion. This motion, diffusion, is given by:

$$D = k_B T / \gamma \quad (2.18)$$

In Eq. 2.15, the force arising from the damping term is given by:

$$\vec{F} = -\gamma \vec{v} \quad (2.19)$$

The drag force experienced by a spherical particle depends on its radius, R , through:

$$\vec{F} = -6\pi\eta R\vec{v} \quad (2.20)$$

such that:

$$\gamma = 6\pi\eta R \quad (2.21)$$

where D is the diffusion coefficient, γ is the friction coefficient, k_B denotes the Boltzmann constant, T the temperature of the system, and η is the viscosity of the solvent.

Drift Velocity

Drift is the process by which a particle moves due to the application of an external force. Here drift velocity is directly related to the strength of the applied force, as well as the friction felt by the particle as it moves through the solvent.

Starting with Eq. 2.15:

$$m\vec{a} = -\nabla U(\vec{x}) - \gamma\vec{v} + \sqrt{2\gamma k_B T}\vec{R}(t) + \vec{F}_{ext} \quad (2.22)$$

the external force is isolated through the following assumptions:

- 1) no particle interaction forces $\therefore -\nabla U(\vec{x}) \Rightarrow 0$
- 2) thermal forces are uncorrelated in time with mean=0 $\therefore \sqrt{2\gamma k_B T}\vec{R}(t) \Rightarrow 0$
- 3) the system is overdamped $\therefore m\vec{a} \Rightarrow 0$

Eq. 2.15 is thus reduced to the following:

$$m\vec{a} = -\nabla U(\vec{x}) - \gamma\vec{v} + \sqrt{2\gamma k_B T}\vec{R}(t) + \vec{F}_{ext} \quad (2.23)$$

$$0 = -\gamma\vec{v} + \vec{F}_{ext} \quad (2.24)$$

$$\gamma\vec{v} = \vec{F}_{ext} \quad (2.25)$$

Thus, in an overdamped system, such as with the Langevin dynamics used here, the drift velocity of a particle is given by:

$$\vec{F}_{ext} = \gamma \vec{v}_D \quad (2.26)$$

$$\vec{v}_D = \frac{\vec{F}_{ext}}{\gamma} \quad (2.27)$$

where \vec{v}_D is the drift velocity, \vec{F}_{ext} is the driving force, and γ is the friction coefficient of the object, as defined in Eq. 2.21.

2.3 Tension Propagation

Fig. 2.7 illustrates the tension-propagation (TP) process. When a polymer is captured by a nanopore, threads, and then begins translocation, TP theory states that a tension front will emerge along the polymer at a distance x from the nanopore. This front demarcates the point at which a relatively relaxed polymer diffusing towards a nanopore transitions into the high field regions near the nanopore. Here, any monomer under the influence of the field effects will uncurl from an initial coiled configuration and move towards the nanopore. Fig. 2.7 illustrates TP progression starting from an initial captured state through translocation. Notice how the TP front propagates as the polymer is pulled towards the nanopore and tension is propagated along the length of the chain.

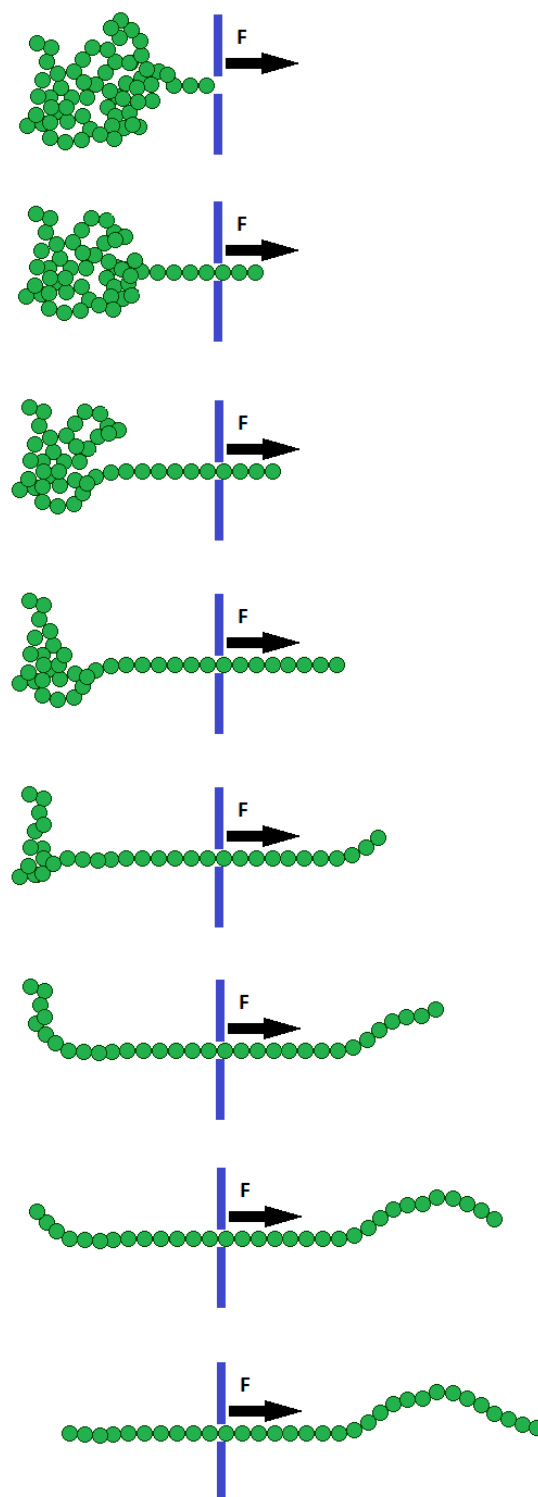


FIGURE 2.7: The propagation of tension along a polymer chain as the polymer is pulled in and through the nanopore during translocation.

Chapter 3

LITERATURE REVIEW

3.1 Introduction

Polymer science is a rich field of research [94, 31, 89, 7, 6, 17, 46, 54, 9, 37, 38, 71, 15, 90, 14, 45, 67, 87, 64, 57, 69, 60, 40, 32, 39, 81, 95, 58, 13, 2, 85, 53, 59, 26, 25, 63, 86, 56, 27, 8, 93, 82, 61, 78, 70, 62, 49, 33, 80, 5, 79, 18, 41, 43, 73, 76, 77, 19, 75, 42, 72, 44, 65, 52, 11, 51, 47, 83, 4, 23, 12, 35, 34, 91, 10, 1, 74, 16, 84, 68, 55, 92, 3, 88, 24] with many problems left unanswered. As new questions arise continuously, a collaborative approach to solutions is almost always necessary. Accordingly, significant progress tends to emerge when theoretical models and experimental work are closely tied together. Although computational models have been around for the last half century, much work is still required to correctly reproduce experimental results or even just to evaluate the proposed theoretical models. Thus, a comprehensive literature review will necessarily include work from both experimental and theoretical groups, fabrication and engineering characterization, and computational and simulation research.

3.1.1 Foundation

Polymer science, a subset of soft matter studies, is largely concerned with structural deformation caused by thermal fluctuations, particularly as it pertains to the movement or conformational changes of a polymer. Here scaling concepts that are applicable to large ranges in polymer size are highly valued as many physical properties of a polymer are dependent on the length of the polymer chain. One such property, the radius of gyration- which is a measure of a polymer's average coil size, has been shown to exhibit a power law relationship to the polymer length. A brief introduction to the foundational aspects of polymer science is now provided.

Nobel Lecture: Spatial Configurations of Macromolecular Chains [21]

In 1974, Paul Flory won the Nobel Prize in Chemistry for his experimental and theoretical contributions in physical chemistry regarding macromolecular behaviour. Considered the founder of polymer science, Flory quantified the concept of excluded volume interactions in polymer chains and, as a result of these interactions, demonstrated how a polymer's configuration would necessarily expand. Among his achievements, Flory also lends his name to an important exponent, ν . This 'Flory Exponent' is often used in polymer science to relate the size of a polymer, R , to its length, N . This is known as the 'infamous' polymer scaling relationship. This power law relation between the polymer's size and length is central to polymer research and is fundamental in the translocation scaling work in this thesis.

Furthermore, it was Flory's realization that the chemical bonds in macromolecules were nearly indistinguishable from those in smaller monomeric compounds, that led to his questioning of the unique properties of certain polymers.

If chemical bonds were not to blame, then what was? He considered perhaps, it was the macromolecules themselves, specifically, the attributes of a long molecular chain. And with that, a lifetime of work began on characterizing polymers and their many configurations, with Flory contributing two fundamental books to his field of polymer science: *Principles of Polymer Chemistry* [20] and *Statistical Mechanics of Chain Molecules* [22].

Nobel Lecture: Soft Matter [30]

In 1991, Pierre-Gilles de Gennes won the Nobel Prize in Physics for his earlier work in which he discovered the concept of scaling as it pertained to polymers. Considered the founder of soft matter research, he demonstrated that the methods for studying order in simple systems could be generalized to more complex forms of matter, particularly polymers. Charging soft matter as being the study of matter which is both complex and flexible, de Gennes was active in many areas, driven to relate the small to the large.

He made notable contributions to the fields of polymers, surfactants, and liquid crystals. Initially working in the field of magnetism, he produced theoretical models of magnetic moment coupling and fluctuations of local magnetization, among many other contributions. It was this initial work in magnetism that allowed de Gennes to draw parallels to the world of polymers. By applying his theory on phase transitions and his concept of how a system behaves when transitioning from order to disorder to describe a wide breadth of fields, he demonstrated that these rules were obeyed in broad generality. Thus, the challenge of describing the many conformations and complex behaviour of polymers was reduced to a certainty that there would be scaling laws to define

these polymer dynamics. Much of this work is contained in his book, *Scaling Concepts in Polymer Physics* [29].

Passive Entry of a DNA Molecule into a Small Pore [28]

In 1999, de Gennes contributed a short analytical model of a DNA chain drifting into a single pore, of radius r_p , that opens only for a brief amount of time. He was interested in determining how much of the DNA chain could enter the pore during this short time frame. He focused on defining three time scales: the average time that passes to be sure a chain has reached the pore, τ_r , the time for the polymer to enter the pore, τ_e , and the time for the whole chain to slide through the pore, τ_s . de Gennes determined that if the polymer's end is located favourable just outside the pore, then the time it will take to enter the pore, τ_e , is given by the pore radius divided by the forward velocity of the polymer. Although nearly 20 years have passed since this work was published, a clear parallel can be drawn to the most recent efforts in polymer translocation, including the focus of this thesis: the capture-translocation process. Here de Gennes' τ_r is comparable to the capture time, τ_e is comparable to the threading time, and τ_s to the translocation time.

Clearly, the conceptual basis of including information regarding the polymer's behaviour *as it approaches the pore* was understood to be an important factor in determining *how* it would pass through. In his own words, "It is seen clearly that the bottleneck is at the entry", de Gennes predicts one of the findings in this thesis where, in a diffusion dominated system, the polymer can often spend the majority of its time threading the nanopore.

3.1.2 Experimental Work

Experimental translocation research can be separated into two core branches: the use of natural nanopores, such as pores that form in the phospholipid bilayers of biological cells; and the use of fabricated nanopores, such as the silicon nitride solid-state nanopores often used for DNA sequencing. Through careful design, experiments can be controlled and effects on translocation observed. For example, consider how changing the solvent salt concentration on one or both sides of the nanopore might affect the translocation time of a charged polymer. One might also be curious to know if this effect strengthened or weakened for longer polymers- possibly leading to a new theory. An interesting biological discovery was also found in viruses- viral DNA can be injected via translocation into a host cell. Experiments are also useful for validating existing theoretical models, again reinforcing the collaborative nature of this field. A selection of experimental work done over the last decade is now provided.

Probing Single DNA Molecule Transport Using Fabricated Nanopores [14]

In 2004, Chen, P. et al. used fabricated nanopores in silicon nitride to study dsDNA electrophoretic transport dynamics. In order to characterize a broad range of molecules under a wider range of conditions Chen et al. reasoned that Si_3N_4 , a relatively inert and thermodynamically stable compound, would better suit the research objective than would a self-assembling protein pore in a lipid membrane. Commenting on prior experimental work, Chen et al. describes how most contemporary work uses standard α - *Hemolysin* proteins to form nanopores which inhibits the collection of detailed signals during translocation due to complex charge distributions and the natural structure of the channel.

Chen et al. identified translocation events based on the current signal recorded (i.e., different types of translocation events would have different signal signatures). Thus, they identified whether the translocation event was of dsDNA moving in single file, or dsDNA chains translocating while folded in on themselves.

Relevant to the work in this thesis, a key finding of Chen et al. is that they observed a greater number of the single-file translocation events at higher applied voltages. They reasoned that because the potential gradient becomes stronger close to the pore, it would necessarily uncurl the dsDNA, thus promoting single-file translocation. They found this to be consistent with observations of shorter dsDNA chains showing far fewer folded-chain translocations, as the entire chain was more likely to be completely uncurled.

Chen et al. also observed that the capture rate for dsDNA by the pore consistently produced a rate that increased linearly with an increase in the applied voltage. This is a particularly useful result; it defines the behaviour of dsDNA capture to be a (thermal) diffusion-limited process. The capture rate, R , of a perfectly absorbing hemisphere of radius r is defined in Eq. 3.1:

$$R_{theory} = 2\pi CDr \quad (3.1)$$

where D identifies the diffusion constant, C the molar concentration, and where r , the capture radius, is both a function of the pore radius and is linearly proportional to the electric field. Therefore, if the diffusion of dsDNA into the absorbing region is assumed to be the rate-limiting step, then the capture rate should be proportional to the applied voltage: $R \sim V_{applied}$.

Note that the capture rate is also defined, and measured by:

$$R_{experiment} = \frac{N_{DNA}}{t} \quad (3.2)$$

where N_{DNA} is the number of dsDNA molecules that have translocated per unit time, t . In fact, the translocation results observed for $R_{experiment}$ do scale linearly with $V_{applied}$, confirming the diffusion-limited behaviour of dsDNA capture.

Fast DNA Translocation through a Solid-State Nanopore [87]

In 2005, Storm et al. studied the translocation of dsDNA through a fabricated silicon oxide nanopore. Varying lengths of the dsDNA were electrophoretically driven through the pore and ionic conductivity signals were recorded for the translocation times. For analysis of the passage times, Storm et al. only recorded the linear, unfolded, translocation events. They recovered a power-law scaling of the dwell time, τ , with length, L_o , of the dsDNA:

$$\tau \sim L_o^\alpha \quad (3.3)$$

here dwell time is synonymous with the translocation time.

Equal concentrations of at least six different dsDNA lengths were sampled, and, applying a least-squares fit to their data, they produce the scaling exponent: $\alpha = 1.27 \pm 0.03$. Performing two additional independent experiments, Storm et al. successfully reproduced this scaling relation, $\tau(L_o)$. The rigorous affirmation of the non-linear result was required because the exponent Storm et al. produced was quite different than the exponents reported in all translocation studies using $\alpha - Hemolysin$ nanopores.

Turning to theory, Storm et al. sought to explain the results of their experiment. They identified that the translocation process consists of two separate stages, capture and translocation. As the dsDNA chain can only reach the nanopore by diffusion, the capture stage is considered a stochastic process, which is not focused on by Storm et al. Instead, they focus on the translocation process, where they quantify the start when an end has entered the pore, and the finish when all of the dsDNA has passed through the pore. Initially captured at time $t = 0$, a polymer of length N will start translocation partially threaded into the pore.

$$\tau \sim R_g^2 \quad (3.4)$$

$$R_g \sim L_o^\nu \quad (3.5)$$

Validating their experimental results, Storm et al. demonstrates how the equilibrium condition for their experiment can be best described by Eq. 3.5, and so using Eq. 3.4 the power-law relation between the contour length and dwell time becomes: $\tau = L_o^{2\nu}$. Using an experimental value for the Flory exponent $\nu = 0.61$ they recover $\alpha = 1.22$, and is in agreement with the experimental value of $\alpha = 1.27 \pm 0.03$, providing one of the first full analyses of translocation through a fabricated nanopore.

Statistics of DNA Capture by a Solid-State Nanopore [66]

In 2013, Mihovilovic, Hagerty and Stein use a solid-state nanopore to electrophoretically capture DNA molecules. An $8nm$ -wide pore permitted the DNA to fold and form hairpins as it was captured for translocation. This behaviour was registered as a disruption of the ionic current readings when the polymer

blocked the pore in varying configurations. Mihovilovic, Hagerty and Stein were interested in quantifying the behaviour of capture- at the time there was not yet a model to describe the distribution of x , the position along a polymer where the polymer is most likely to be captured. Prior work had suggested opposing views, either folds along the polymer would occur at equal probabilities but that it was energetically more favourable to be caught in an extended configuration and by an end[87], or there was a bias for unfolded polymers that increased with applied voltage such that the molecules would pre-align outside the pore along the field lines prior to capture[13].

Mihovilovic, Hagerty and Stein comment that the strong bias for capturing polymers on end is a result of the configurational entropy of the approaching polymer and not due to polymers searching for energetically favourable configurations before translocating. Tracking the conformational changes of approaching polymers is one of the core results in this thesis. The assumptions about a polymer's configuration immediately preceding translocation are tested and are related back to the polymer's configuration as it is approaching the nanopore for capture. Of interest is that these initial configurations can be controlled (in some manner) by altering the drift-diffusion balance of the system.

Polymer Capture by α - Hemolysin Pore upon Salt Concentration Gradient [44]

In 2014, Jeon and Muthukumar used an α - Hemolysin protein pore to measure the capture rate of single sodium poly(styrene sulfonate) molecules. Three experimental parameters were varied for the analysis: the applied voltage, the

pH, and the salt concentration asymmetry across the pore. As with all experimental translocation studies, the current through the protein pore is recorded and a blockage event is counted as a capture event if the current drops below 75% of the open pore current.

At the time, there was yet to be a theoretical model which could describe coupled forces under nonequilibrium conditions, such as those observed in the experiment. Nevertheless, the work put forth by Jeon and Muthukumar was successful in validating the idea that capture may be influenced by imposing nonequilibrium drift conditions. The computational model developed for this thesis necessarily probes this relationship between drift and diffusion.

3.1.3 Theoretical Work

Within polymer science, the theoretical understanding and model building of translocation is of interest. The value in understanding the dynamics of this transport process is substantial; both for biological comprehension and for nanoscale fabrication where the controlled (natural or forced) movement of a polymer is required. Conceptual and statistical models that describe and predict experimental work suggest possible universal scaling laws. They also suggest the effects of varying system conditions, such as chemical potential gradients, energy barriers to translocation, and solvent conditions. Here, a collection of early theoretical work on polymer translocation provides a basis from which the field has grown.

Polymer Translocation through a Pore in a Membrane [89]

In 1996, Sung and Park developed one of the first comprehensive analytical models of polymer translocation. By treating translocation as a stochastic process, they first quantified an energy barrier to translocation which was dependent on the polymer length, N , the number of segments of the chain on both sides of the nanopore, and the chemical potential per segment of both *cis* and *trans* sides. Sung and Park assume the chain diffusivity, D , remains constant during translocation such that $D = k_B T / \gamma \sim 1/N^\nu$ where γ is the chain friction proportional to N^ν . Here ν takes on the value of 1 if hydrodynamics interactions are neglected, or 1/2 if they are included. What is significant about their work is that by incorporating the three-dimensional chain conformations and associated flexibility and entropy they were able to show that the chain flexibility would significantly slow translocation. Additionally, if chaperone chemicals are present on the *trans* side (which bind to segments along the polymer chain and prevent backwards diffusion), then the flexibility of the polymer on the *trans* side decreases, and the rate at which the polymer is translocating increases. Thus, Sung and Park demonstrated that the global translocation dynamics are independent of the local potential barriers and the translocation time, τ , can be described for long polymers by:

$$\tau \sim \frac{L^2}{2D} \quad (3.6)$$

If $D \sim 1/N$ then $\tau \sim N^3$ and if $D \sim 1/N^{1/2}$ then $\tau \sim N^{5/2}$, thus providing time scaling for polymer translocation models with or without hydrodynamics.

Polymer Translocation through a Hole [71]

In 1999, Muthukumar expanded the model proposed by Sung and Park to demonstrate that by incorporating details of the hole (pore; nanopore) a parametrization of the rate constant, k_0 , was possible. Here k_0 is the rate for transporting a monomer across the hole, and is independent of polymer length, N . Thus, for symmetric barriers, Muthukumar presents the translocation time, τ as:

$$k_0\tau = \alpha N^2 \quad (3.7)$$

where α is a constant reflecting the chemical potential on either side of the nanopore.

In the absence of a chemical potential gradient Muthukumar finds $\tau \sim N^2$. For asymmetric barriers where translocation is against the chemical potential gradient Muthukumar has $\tau \sim \exp(N)$. For translocation along negative chemical potential barriers (i.e., favourable translocation) $\tau \sim N$ where $\tau \sim N(T/k_0\mu)$ for large $N\Delta\mu/T$ and $\tau \sim N/k_0$ for small $N\Delta\mu/T$. Here T is the temperature. What Muthukumar contributed with this model was to provide a means to quantify the particular effects a pore might have on translocation. Thus, k_0 reflects a temperature dependent rate assumed to depend on the interaction of a monomer and the pore proteins. The ability to quantify pore effects on translocation is invaluable for building accurate computational models such as those designed for this thesis.

Anomalous Dynamics of Translocation [15]

In 2001, Chuang, Kantor and Kardar used numerical simulations to simulate both one- and two-dimensional polymer chains (length N). Common theoretical models at the time assumed quasistatic dynamics and predicted an unforced translocation time, τ_{trans} , that scales as N^α , where $\alpha = 2$. In quasistatic dynamics the relaxation time is considered to be less than the translocation time, that is, $\tau_R < \tau_{trans}$. However, through simulations of different polymer lengths, Chuang, Kantor and Kardar uncovered that for the translocation process, α approaches an asymptotic limit that is larger than 2. Here, their simulations indicated that the assumption of quasistatic in earlier work was incompatible for excluded volume effects of long polymer chains. Note that excluded volume interactions are included to prevent a polymer chain from passing through itself in the simulation; the monomers will gently repel those that are not bonded to it to simulate a more realistic scenario.

The Rouse relaxation time, τ_R is predicted by:

$$\tau_R \sim N^{1+2\nu} \quad (3.8)$$

With $\nu = 3/4$ for self-avoiding chains in two-dimensions, the relaxation time becomes $\tau_R \sim N^{2.5}$, significantly larger than the quasistatic $\tau_{trans} \sim N^2$. Here Chuang, Kantor and Kardar make the connection that translocation across a barrier must at least require the polymer to diffuse a distance equal to its radius of gyration. Thus, when compared to idealized models that do not consider excluded volume interactions, the relaxation time is necessarily longer, and the Rouse relaxation time scale should instead reflect the lower limit of the translocation time. Therefore, Chuang, Kantor and Kardar conclude that translocation

is indicative of *anomalous* dynamics. The extension to three-dimensional dynamics, such as the focus of this thesis, includes an additional dimension of movement and diffusion for the polymer.

3.1.4 Simulation Work

Translocation research will often use computational models to evaluate the theoretical framework and reproducibility of experiment outcomes ([17, 63, 24, 8, 46, 54, 36, 9]) or solely to understand the process itself. More recently, polymer translocation work has benefited from software packages that allow controlled visualizations of the process, as well as turning to high performance computing methods to more quickly produce thousands of simulated translocation events. Simulations, therefore, have the potential to give unique insight and allow the evaluation of many possible outcomes to assist in fine tuning future experiments for efficiency and reliability. Below, several simulation results are explored.

Dynamical Scaling Exponents for Polymer Translocation through a Nanopore [63]

In 2008, Luo et al. sought to resolve discrepancies in literature centered around the scaling exponent and scaling law of translocation time τ as a function of N through the familiar power-law relation: $\tau \sim N^\alpha$. Luo et al. set several 2D and 3D models for simulating both driven and unbiased polymer translocation for various polymer lengths, $15 \leq N \leq 800$. Luo et al. found that for unbiased translocation, in both 2D and 3D, $\alpha = 1 + 2\nu$. For driven polymer translocation in 2D there is a crossover from short to long N that is reflected in $\alpha \approx 2\nu$ for $N \leq 200$ which flips to $\alpha \approx 1 + \nu$ for long N . For driven translocation in 3D,

the crossover vanishes yet $2\nu < \alpha = 1.42 < 1 + \nu$ for $N \approx 40 - 800$. Luo et al. considered if the crossover region might be found at even larger N than simulated here because the nonequilibrium effects should be more pronounced in 3D.

Scaling Exponents of Forced Polymer Translocation through a Nanopore [8]

In 2009, Bhattacharya et al. performed three-dimensional Langevin dynamic simulations of forced polymer translocation. They were interested in the scaling dependence of the polymer chain length, N , and used the average velocity, v_{cm} , of the polymer's center of mass during translocation to quantify the process. Bhattacharya et al. also evaluated the radius of gyration, R_g , and found that there was a dependence in the scaling exponent on the nanopore geometry. Bhattacharya et al. observed that the shape of the polymer chain changed substantially during translocation, and found the translocation time to vary as:

$$\tau \sim N^\alpha \quad (3.9)$$

$$\langle \tau \rangle \sim \frac{\langle R_g \rangle}{\langle v_{cm} \rangle} \quad (3.10)$$

where α is the scaling exponent.

Bhattacharya et al. identified how boundaries on scaling exponents may arise from conformational changes in the polymer due to chain length and the time dependent quantities. Testing on both a triangular and square lattice, Bhattacharya et al. found their results to remain consistent with current theoretical models indicating geometric dependencies of the pore width. By performing numerous simulations on a wide range of polymer lengths, Bhattacharya et al.

provided a basis of relating conformational changes in the polymer to the passage time of nanopore translocation.

Memory Effects During the Unbiased Translocation of a Polymer through a Nanopore [36]

In 2012, de Haan and Slater performed unbiased translocation simulations using Langevin dynamics to determine if forward and backward motion of a polymer was correlated to solvent viscosity. de Haan and Slater found that at short time scales forward-correlated motion was most likely related to the inertial term in the equation of motion. They also demonstrated that beyond short time scales the polymer's motion would be affected primarily from the solvent viscosity. For low viscosity solvents, the net motion of the polymer would continue forward due to a lack of damping, whereas high viscosity solvents would induce a backward correlation of the polymer's movement, emphasizing the relevance of polymer motion prior to translocation.

3.1.5 Tension Propagation and Capture Process

Apart from the translocation process itself, this thesis explores the drift-diffusion balance of the simulated system as a whole, and specifically the dynamics involved in the capture process of the polymer, and the resulting propagation of tension along the chain arising from competing thermal and electrical forces. Thought to compress and elongate the polymer, these conformational changes would then oppose one of the fundamental assumptions in the majority of coarse-grained simulations of polymer translocation: the polymer begins translocation in a relaxed, equilibrated state. The simulation of the capture process has been developed in limited detail and therefore few contemporary groups

exploring this phenomenon through computational models exist. Relevant theoretical, experimental, and computation models are provided as they relate to the simulation methodology of the capture process developed here.

Nonequilibrium Dynamics of Polymer Translocation and Straightening [81]

In 2007, Sakaue produced an analytical model to describe the absorption of a polymer by a hole and identifies polymer translocation as being one of the most relevant cases of polymer stretching due to an externally imposed velocity gradient. The model begins by assuming a polymer has arrived by an end to an attractive hole. Here, the first monomer will be pulled strongly, which will affect the monomers in its immediate rear vicinity, but not those further along the chain. This subunit of initial monomers being pulled will start to move with an average velocity reflected by the velocity gradient near the hole. Conceptually, this motion gives rise to an interface where the monomers attracted to the nanopore cross into a region of 'strong' absorption from their initial position of equilibration at rest.

Sakaue concludes that an externally imposed velocity gradient (i.e., the nanopore absorption) can exceed the inverse relaxation time for long polymers. Thus the rate at which the polymer is absorbed into the nanopore is faster than the time it takes for the polymer to relax. Fig. 3.1 illustrates how it is possible for a polymer to be absorbed by the nanopore faster than it can relax, and resembles the behaviour of biased translocation events.

Dynamical Diagram and Scaling in Polymer Driven Translocation [79]

In 2011, Saito and Sakaue proposed a dynamical scaling model that applies to most polymer translocation scenarios found in literature. They developed a

more comprehensive picture for tension-propagation physics as it pertains to driven translocation. The goal was to expand current theory to cover a greater range of parameters arising from distinct nonequilibrium conformations of real experiments. The key discovery of the work here by Saito and Sakaue was that finite-size effects play a crucial role when attempting to compare experiment to simulation, and, apart from a near-equilibrium regime, Saito and Sakaue find three distinct additional nonequilibrium regimes- each with a unique scaling exponent.

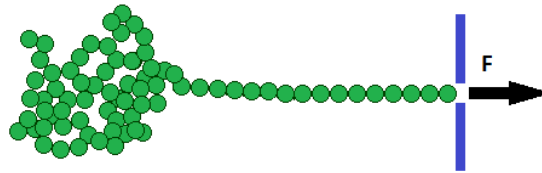


FIGURE 3.1: On-end elongation typical of the capture process under tuned P conditions.

The path of tension-propagation theory emphasizes that an event will first begin in the equilibrium state, then progress into one of three tension-propagation states. Dictated by the force felt and configuration of the polymer, one regime may emerge as the dominant scenario. In between these two tension-propagation regimes lies a boundary, or cross-over, regime. Saito and Sakaue propose that perhaps there are in fact many different regimes and the finite-size effects may make it hard to obtain an accurate exponent. They quantify the translocation time as being perhaps a combination of each regimes' effect.

For the work done in this thesis, tension-propagation effects are emphasized when simulating the capture of the polymer under suppressed diffusion conditions. Fig. 3.1 illustrates the propagation of tension along a polymer chain.

Here the extension of monomers that are being pulled into the nanopore contrast those which have not yet felt the field effects and remain in an initial, more relaxed configuration.

Chain Deformation in Translocation Phenomena [19]

In 2012, Farahpour et al. looked at the deformation of ssDNA as it is captured and pulled into the pore. Capture occurs at a distance of r_{cap} from the pore, and identifies where the electric field gradients sharply increase towards the pore, facilitating translocation.

First proposed by Kowalczyk et al. [49], an oblate spheroidal coordinate system was used to solve the following Laplace equation in 3D:

$$\nabla^2 V = \sum_{i=1}^3 \frac{\partial^2 \Phi(\mu, \nu, \phi)}{\partial u_i^2} \quad (3.11)$$

An oblate spheroidal coordinate system has two sets of curvilinear coordinates obtained by revolving elliptical cylindrical coordinates about one axis, and a third set of coordinates that are planes passing through the same axis. This coordinate system successfully describes the electric potential as a function of the pore shape and the applied voltage. Farahpour et al. adapts this method for simulations by setting the electrodes at infinity and assumes that a one-sheeted hyperboloid with $\nu = \nu_0$ may be substituted for the pore (radius a) and membrane wall (length l). Here ν is an arbitrarily small value, $\nu \ll \pi/2$, and is obtained via $\nu_0 = \cos^{-1}(a/c)$, where c is the radius of the focal ring of the coordinate system. Forcing $a > l$, the solved Laplace equation will yield an expression for a continuous electric potential over all space:

$$\Phi(\mu, \nu, \phi) = \frac{V_0}{\pi} \tan^{-1}(\sinh \mu) \quad (3.12)$$

where (μ, ν, ϕ) are the oblate spheroidal coordinates, and V_0 is the potential drop across the system and $\mu \in (-\infty, +\infty)$, $\nu \in [0, \pi]$, $\phi \in [0, 2\pi]$. The oblate spheroidal coordinates map to cylindrical ones through the following relations:
 $\rho = c \cosh \mu \cos \nu$; $z = c \sinh \mu \sin \nu$; $\phi = \phi$.

Fig. 3.2 and Fig. 3.3 illustrate the oblate spheroidal coordinate system.

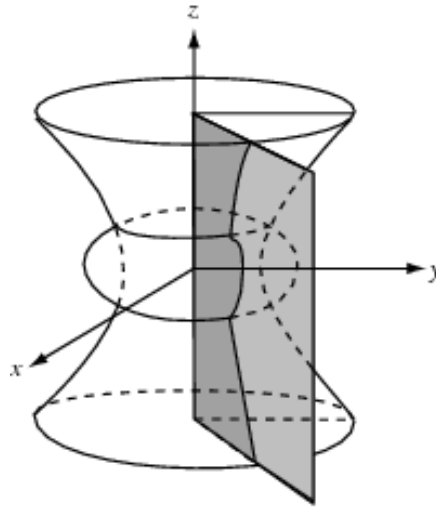


FIGURE 3.2: The revolution of elliptical cylindrical coordinates form two of the coordinates in an oblate spheroidal coordinate system [96].

By analytically solving for this electric field, both inside and outside the pore, Farahpour et al. created a more realistic situation for capture, with the field converging into the pore on the *cis* side and diverging out from the *trans* side. This also led to the prediction that any charged polymer close enough to be captured, would necessarily become elongated as it is pulled unevenly towards the pore. To test this assumption Farahpour et al. performed simulations using hybrid lattice Boltzmann-molecular dynamics (LB-MD) such that long range hydrodynamic interactions as well as electrostatics could be included on

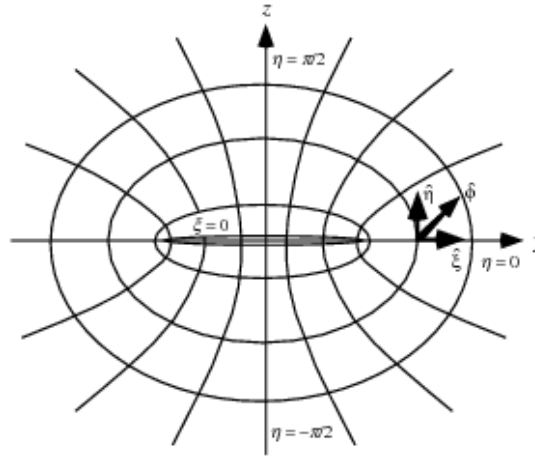


FIGURE 3.3: The third set of coordinates in an oblate spheroidal coordinate system consists of planes passing through the axis depicted in Fig. 3.2. A sample plane is shown [96].

the short polymers ($N = 10-60$). When the simulation begins the polymer is positioned along the pore's axis, a distance of r_{cap} from the pore's mouth. Here, the polymer is left to equilibrate until it is fully relaxed, at which point the applied electric field is turned on and the capture process begins. Once sufficient samples were recorded for each polymer of length N , Farahpour et al. identified that there are two forces at play: an electrophoretic force acting on the charged monomers; and the non-uniform nature of the electric field depending on the distance from the pore. Both force effects were found to elongate the polymer.

Electrophoresis of DNA Coil Near a Nanopore [76]

In 2013, Rowghanian and Grosberg developed an analytical model to describe the electrophoretic flow of a solvent around a long rigid polymer. Focusing on the solvent effects near the mouth of a nanopore during capture and translocation, this mathematical analysis provided a rigorously solved model for a plausible explanation of the effects of an external field on the solvent's motion.

Rowghanian and Grosberg based the behaviour of the solvent on that of an elongated jet, or 'flow-field', which is modelled after a thin jet injecting momentum into a liquid. They were successful at describing how an electrophoretic flow will circulate around a coiled polymer as it translocates through a nanopore. Rowghanian and Grosberg outlined how changes in the applied field provide a source of momentum for the solvent and the model replicates the size-independent electrophoretic mobility found in experiment.

Electrophoretic Capture of a DNA Chain into a Nanopore [77]

In 2013, Rowghanian and Grosberg used the theoretical model they developed regarding the electrophoretic flow of a solvent near a nanopore and expanded it to detail the capture process of a polymer as it moves through an externally applied field. Rowghanian and Grosberg reproduced the diffusion limited and barrier limited regimes previously observed in experiment during the capture process. They find that the data fit indicates the capture rate increases with N to the power $\alpha = 1.03 \pm 0.16$. They mention that the experimental data collected may have been from a region where crossover from barrier-limited to diffusion-limited regimes occurred. Their methodology is important to the work in this thesis as the model is one of the first that describes the shape changes of a polymer as it is captured by a nanopore for translocation.

Chapter 4

SIMULATION APPROACH

4.1 Translocation Conditions

4.1.1 Nanopore

For all translocation dynamics simulated in this work, a cylindrical nanopore was modelled with an effective pore diameter of $\approx 1.4\sigma$ and a length of $\approx 1\sigma$. With an effective diameter slightly smaller than the width of 1.5 monomers, single-file translocation is forced and must occur by one of the polymer's two ends.

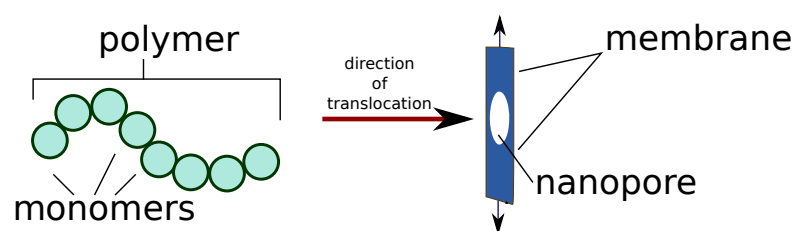


FIGURE 4.1: A schematic of the nanopore system used for simulations.

The nanopore resides at the center of an impenetrable 'membrane', and is positioned at the center of the simulation environment. Fig. 4.1 provides a schematic of the simplified system. Here translocation occurs when a polymer

passes from the *cis* side of the nanopore, through the nanopore, and exits on the nanopore's *trans* side. The membrane is not made up of simulation monomers, but rather it is quantified by the excluded volume and repulsion potential. It spans the entire plane orthogonal to the nanopore's axis and is $\approx 1\sigma$ in length along this axis.

4.1.2 External Field

To focus on the dynamics surrounding the capture of the polymer by the nanopore and how this affects translocation, it is necessary to include the full electrical effects of the external field outside the nanopore. A finite difference approach was utilized to solve the potential in the system and the resulting field was implemented into the simulations as radial and axial forces. Fig. 4.2 illustrates the applied potential both in and around the nanopore, with the top of the figure corresponding to the *cis* side of the nanopore.

Notice how the potential is flat far from the nanopore on both sides. Most simulations to date consider the applied field to be negligible outside the nanopore and so model a flat potential everywhere but within the nanopore itself. However, Fig. 4.2 clearly shows that there are high field gradients close to the nanopore that will pull the polymer in on the *cis* side and push the polymer out on the *trans* side.

4.1.3 Péclet Number

The drift and diffusive dynamics that arise during translocation must be quantified. Here, drift refers to the directed dynamics -the field effects- that drive the polymer through the system and arise from the potential as calculated for the geometry of the nanopore. The thermal energy of the system is quantified

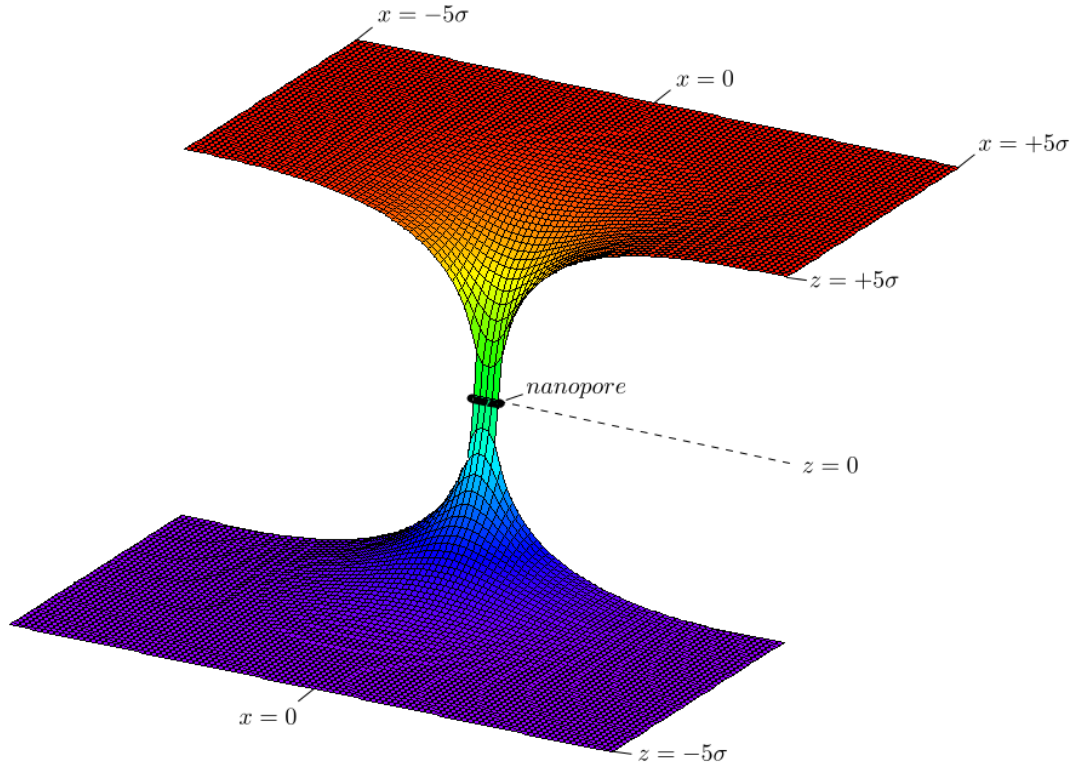


FIGURE 4.2: A cross-section of the external potential applied to the system. The center of the nanopore is located at $[x \ y \ z]=[200 \ 200 \ 200]$.

by $k_B T$, where k_B denotes the Boltzmann constant and T is the temperature of the system, and describes the diffusive dynamics of the polymer's movement.

The drift-diffusion balance throughout the system is characterized by a dimensionless parameter that describes the relative strength of the thermal energy to the electric field strength. P , the Péclet number, is defined here:

$$P = \frac{vL}{D} \quad (4.1)$$

where v is the drift velocity, L is a characteristic length, and D is the diffusion coefficient. As described earlier, the diffusion coefficient can also be given by

$D = k_B T / \gamma$. Additionally, in an overdamped system, recall the drift velocity, v , can also be given by $v = F / \gamma$ where F is the driving force and γ is the friction coefficient.

Substituting these parameters into Eq. 4.1, the Péclet number can also be defined as:

$$P = \frac{FL}{k_B T} \quad (4.2)$$

where, for the simulation work done here, L , the polymer length, is denoted by N . Therefore, for any polymer length, N , we find that $P \sim F / k_B T$.

The Péclet number can take on a range of values and it has been shown in prior work that altering the temperature of the system is the most appropriate method of choosing different Péclet numbers [34]. Thus selecting different values for $k_B T$ will simulate different Péclet numbers.

In this work two different Péclet numbers were chosen for comparative simulations:

i) a “default Péclet” number: By setting $k_B T = 1.0$ a diffusion-dominated system is created. This is representative of the majority of coarse-grained studies of translocation using ‘default’ parameters. Previous work has demonstrated that this value may over-estimate the thermal component [34].

and

ii) a “tuned Péclet” number: By setting $k_B T = 0.1$ a system where diffusion is suppressed is created. An order of magnitude lower than default P , this value more accurately reflects the drift-diffusion balance as it is more closely ‘tuned’ to experimental conditions [34].

4.2 Simulation Protocols

The translocation of a freely-jointed polymer chain through a nanopore was modelled using a standard coarse-grained approach [86]. Here, two different simulation protocols are used: the standard approach and a newly devised capture approach. At present, most standard simulation methodologies oversimplify the physical conditions of polymer translocation through a nanopore. With this in mind a revised methodology was designed to account not only for the force effects inside the nanopore but also for the physical conditions imposed on the polymer during the capture process- i.e., how the drift-diffusion balance affects the progression of a polymer towards the nanopore.

4.2.1 Standard Protocol

In order to obtain a baseline for the simulation environment, a protocol based on current methodologies was designed. Referred herein as the *standard protocol*, results found in current literature were reproduced such that this methodology may be compared to the newly developed capture simulation protocol.

The standard protocol corresponds to an approach that is typical of the majority of polymer translocation simulation studies. These methodologies assume that any externally applied field is strongest inside the nanopore and quickly dies off on both the *cis* and *trans* sides. They are therefore designed such that any applied field, regardless of geometry, is contained within the nanopore and zero elsewhere. This results in an additional force being applied *only* to the current monomers found within the nanopore at any given time.

Equilibration

In the absence of any applied external field, equilibration of the polymer is achieved with one or more monomers fixed in place within the nanopore. The radius of gyration, R_g , is recorded for both perpendicular, $R_{g\perp}$, and parallel, $R_{g\parallel}$, directions. Here the reference point is the nanopore, where $R_{g\parallel}$ describes the axis running through the nanopore.

Once equilibrated, the fixed monomers are released and the external field is turned on. This forced initial starting condition is unrealistic as it assumes the polymer to start translocation not only in an equilibrated conformation, but also prethreaded in the nanopore.

Translocation

A successful translocation event occurs when a polymer passes through the nanopore and exits on the *trans* side, at which point R_g is again recorded once the last monomer in the chain has left the nanopore. Occasionally the polymer may retract to the *cis* side once released from equilibration. This is treated as a failed translocation event.

4.2.2 Capture Protocol

By focusing on the capture process of a polymer by a nanopore, a newly devised simulation protocol was evolved with the expectation of more closely tying experimental results with current theoretical translocation models. Referred herein as the *capture protocol*, it is an extension of the system devised in [65]. A schematic depicting each phase is provided in Fig. 4.3 and, as with the standard protocol, R_g is recorded at each defining stage. Fig. 4.3 illustrates the

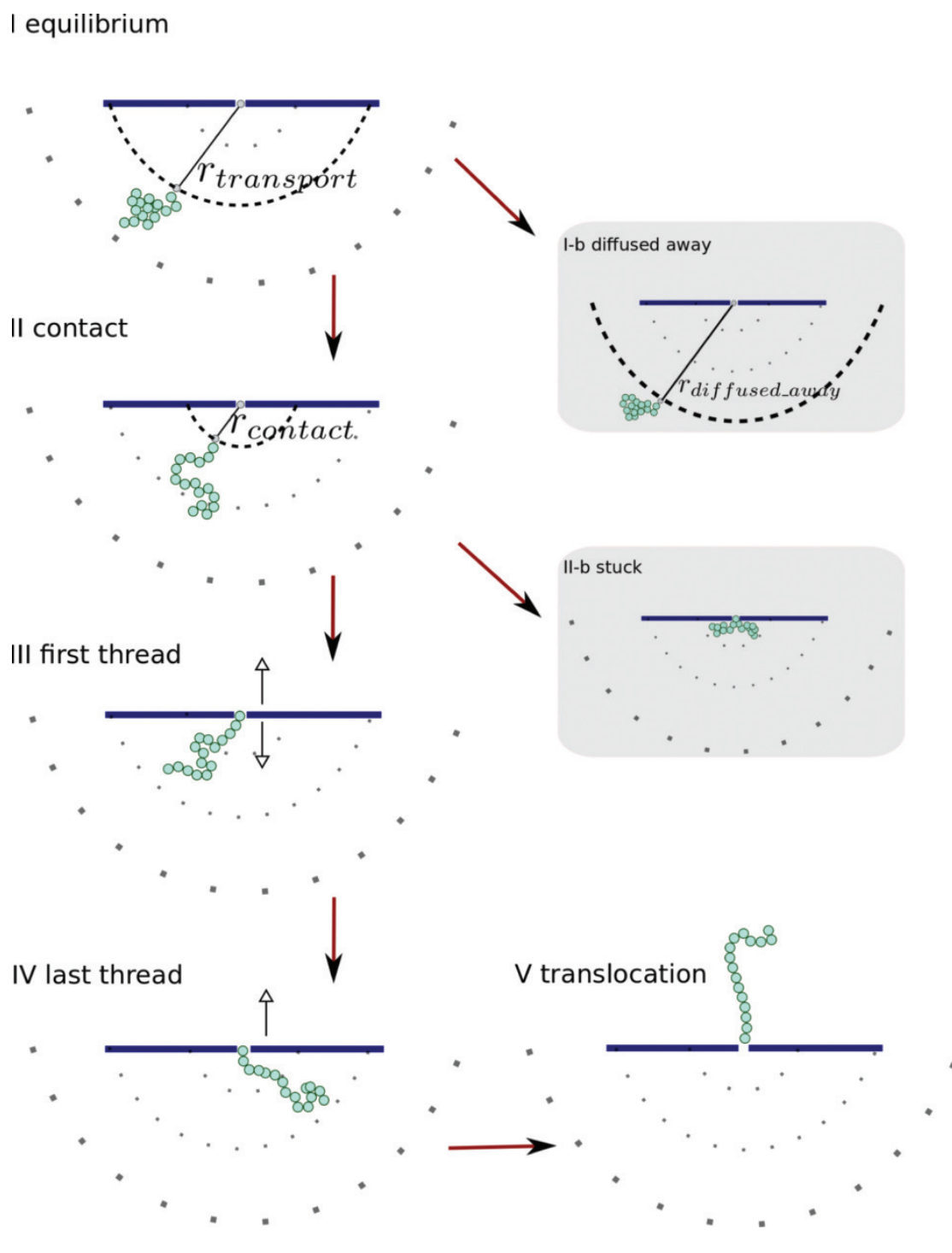


FIGURE 4.3: Schematic representation of the capture protocol. A successful translocation occurs when the polymer passes from I-V. Unsuccessful translocation events will either diffuse away (I-b), or remain stuck (II-b) and unable to thread [92].

full capture-translocation process used in the simulations. All relevant stages discussed are identified.

Equilibration

The polymer is built on the *cis* side of the nanopore with its first monomer placed on a hemisphere a distance of 125σ from the center of the nanopore. This location is regenerated for each independent run of the simulation such that a well-distributed spatial sampling of initial polymer starting coordinates may be tested. The $N/2$ monomer is fixed in place and in the absence of any external field the polymer is left free to equilibrate for a period of time longer than the N -dependent relaxation time. This permits a symmetric relaxation of the polymer and prevents premature biasing towards the same on-end capture that can occur by equilibrating the polymer with an end fixed. (ref. section I in Fig. 4.3).

Transport

In order to simulate the capture process, the polymer must be permitted to diffuse into the high field regions found close to the nanopore. Here, the polymer will cross into a region dominated by drift and be pulled towards the nanopore. Regardless of the system conditions, simulations run at either Péclet number will produce diffusion processes that are naturally quite lengthy. It is not at all unlikely for the polymer to diffuse away from, instead of towards, the nanopore. Thus, in order to favour diffusion *towards* the nanopore, the polymer is transported in its equilibrated configuration closer to the nanopore. The polymer is transported along a radially extending vector that connects the center of the nanopore to the closest monomer. After transportation the monomer will

reside on a hemisphere of distance R_{port} from the center of the nanopore. R_{port} is defined independently for each Péclet condition and identifies a distance at the far extent of the external field profile of suitable trade-off between efficient simulation durations and negligible field effects. For default P $R_{port} = 22$ and for tuned P $R_{port} = 30$.(ref. section I in Fig. 4.3). R_{port} choices are discussed in Sec. 4.3.

Diffused Away

Although the system is tuned to encourage polymer diffusion towards the nanopore, there are still situations in which the polymer will instead diffuse away. If the polymer diffuses too far away from the nanopore it is highly unlikely that the polymer will then return close enough to the nanopore. In this case, the simulation is instead restarted when the closest monomer is found beyond a cutoff distance of 40σ . R_g is not recorded in this case. (ref. section I-b in Fig. 4.3).

Contact

If the polymer instead diffuses toward the nanopore it will diffuse close enough to the nanopore where it is captured by the external field around the nanopore. As the polymer is driven closer to the nanopore it will eventually make contact with the nanopore, which is considered the point at which the polymer 'sees' the nanopore. This is defined at a distance of 2.5σ and is particular to the geometry of the nanopore. Once the closest monomer crosses this boundary, R_g is recorded in order to document the configuration of the polymer as it approaches the nanopore for translocation. Note that contact need not be made by an end monomer. (ref. section II in Fig. 4.3).

Stuck

Under certain simulation conditions the likelihood of the polymer becoming stuck at the nanopore's entrance increases substantially. A stuck event occurs when a polymer is unable to thread into the nanopore on-end. With the external field pushing the polymer towards and against the nanopore and membrane, a polymer, unable to thread for translocation, can remain at the mouth of the nanopore for a long time. Rather than wait for a possible, but unlikely, successful thread event, the simulation is terminated after $3\tau_{Rx}$, where τ_{Rx} is the relaxation time of the polymer. R_g is not recorded. (ref. section II-b in Fig. 4.3).

First Thread

Threading is defined when a polymer is pulled into the nanopore and its leading monomer crosses the axial midway point. The nanopore is sufficiently narrow to force single file translocation and as a result threading will most likely occur by an end. A first thread event is defined by the first occurrence of a monomer crossing this midway point. A parallel may be drawn to the initial setup in the standard protocol where at least one monomer is fixed inside the nanopore. R_g is recorded. (ref. section III in Fig. 4.3).

Last Thread

With the inclusion of the external field, the simulation explores the effects of competing thermal and field forces. This is most evident during threading events, as under certain conditions the thermal effects may be strong enough to pull a threaded polymer back into the *cis* side. However, since the external field is not contained to the inside of the nanopore (as in the standard protocol), but rather extends out beyond the nanopore, field forces can drive the polymer

back towards the nanopore to attempt threading once again. This process of rethreading and retracting may repeat a number of times. If a thread event results in a successful translocation, the event is recorded as the last thread and R_g is recorded. (ref. section IV in Fig. 4.3).

Translocation

Translocation is defined by a polymer passing through the entire length of the nanopore and exiting on the *trans* side. It is directly preceded by the last thread event. Each monomer leaving the nanopore in single-file must cross a distance of 1.0σ from the center point of the nanopore for a successful translocation to be recorded. If successful, R_g is recorded. (ref. section V in Fig. 4.3).

4.3 Additional Considerations

4.3.1 Determination of R_{port}

As discussed, the capture protocol involves transporting the equilibrated polymer to a location that is close enough to the nanopore to favour translocation, yet far enough away not to start in the high field regions. This distance, R_{port} , extends radially outward from the nanopore center and resides on the surface of a 3D hemisphere enclosing the nanopore. To facilitate translocation, simulation constraints aim to maximize computational efficiency, and by choosing an appropriate value for R_{port} , significant reductions in computational time are possible. This is a direct result of the likelihood for any one event to fail by either diffusing away from the nanopore or by becoming stuck, thus triggering an additional translocation event attempt. In addition, to properly model the capture process the polymer cannot be placed too close to the nanopore. The initial

diffusion towards high field regions not only affects the polymer's conformation, it is also central to the work of this thesis which is motivated to identify how the full capture process may alter translocation dynamics in simulations.

To achieve this condition, the initial transportation distance, R_{port} , must be substantially further away from the nanopore under tuned Péclet conditions than R_{port} under default Péclet conditions. Under default Péclet conditions diffusion dominates the system thus the placement of the polymer is not particularly sensitive to the starting location outside the high field region. The polymer quickly relaxes relative to the time it takes to diffuse towards the nanopore. However, under tuned Péclet conditions diffusion is suppressed. This permits the closest section of the polymer to be caught by the high field and driven in towards the nanopore. Under these conditions the polymer is unable to fully relax once caught, and effectively pulls itself monomer-by-monomer towards the nanopore. In both cases, there is a chance for the polymer to become 'stuck' at the entrance of the nanopore when not caught on end, as single-file translocation is required.

The locations of R_{port} were therefore determined via a set of runs testing the effect of gradually increasing the distance of R_{port} for both Péclet conditions. Here a minimum of 2000 successful translocation events were performed for each value of R_{port} . Fig. 4.4 and Fig. 4.5 identify the average rate of failure for polymers at each distance. The values chosen for R_{port} are based off of the $N = 100$ runs. As shown, it is necessary to choose different values of R_{port} for each Péclet number. At default P R_{port} is set to 22, and for tuned P R_{port} is set to 30. Here a balance of failed attempts to successful translocations is achieved while maintaining a statistically relevant sample size of initial polymer configurations.

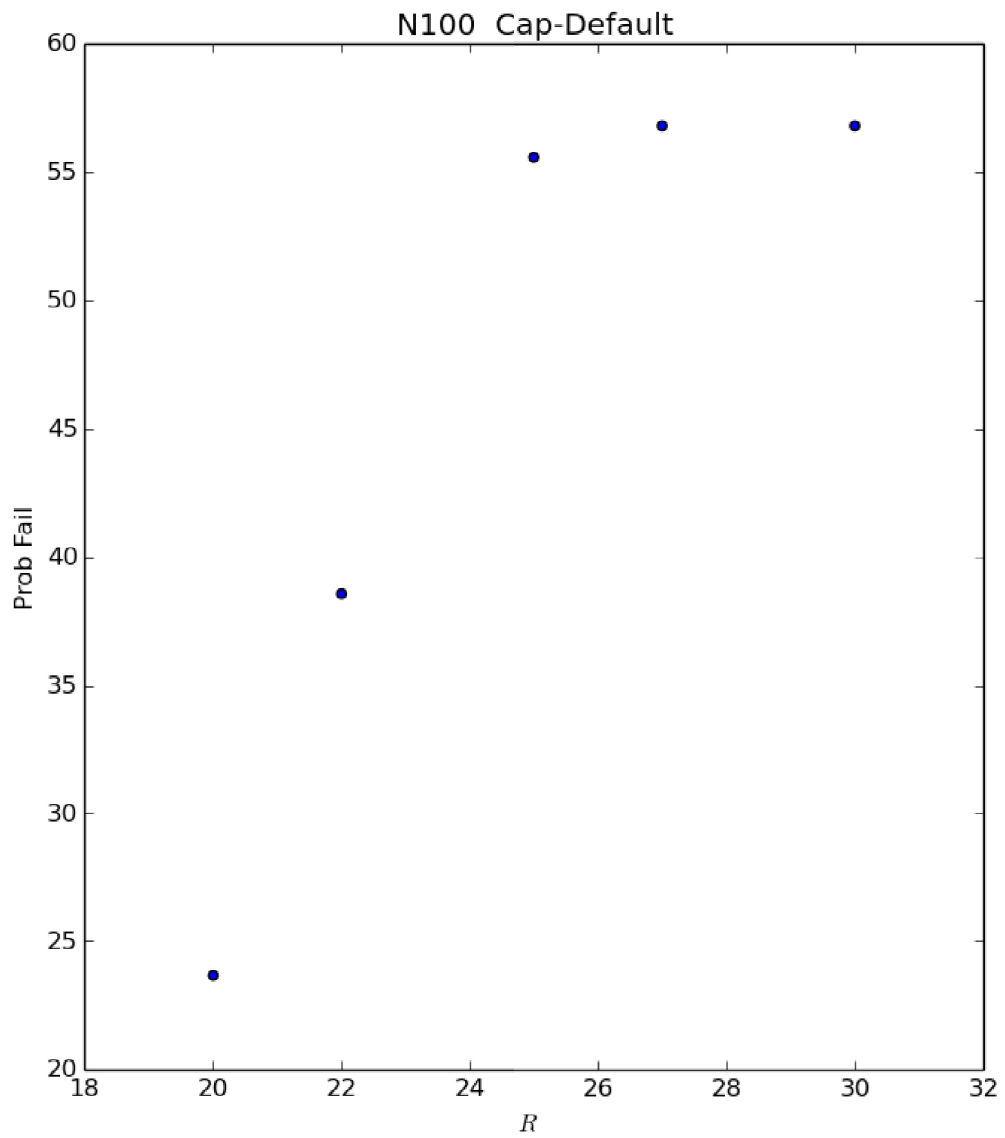


FIGURE 4.4: Event failure rates for five different values of R_{port} . Here $N = 100$ at default P .

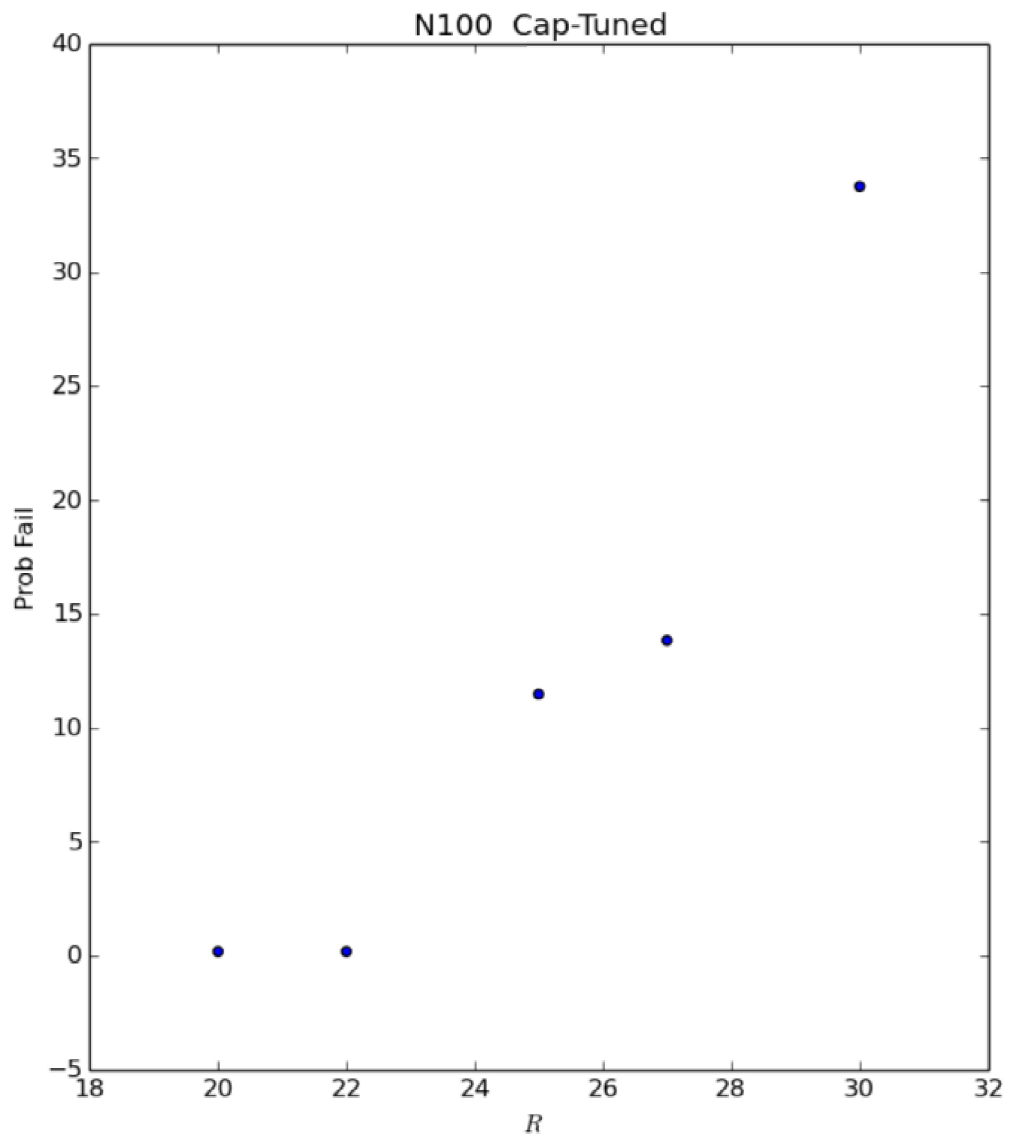


FIGURE 4.5: Event failure rates for five different values of R_{port} . Here $N = 100$ at tuned P .

4.3.2 Computational Details

Software

All polymer translocation simulations used the open-source software package ESPResSo[55]. It is designed for soft-matter research and permits customization of many particle simulations, coarse-grained for molecular dynamic applications, such as the polymers used for translocation in this work. To visualize the translocation events, the modelling and visualization program, VMD [39], provides a graphical interface that allows manipulation and recording of the translocation events. Polymer screen shots in this thesis were obtained from simulations run by ESPResSo and visualized with VMD.

Data

The range of polymer length, N , used ($N=50,100,200$) is sufficient for extracting scaling trends in the work presented here. Simulation runs of translocation for $N=25$ and 300 were run as checks in addition to the standard polymer lengths. The work here is primarily focused on identifying whether or not the capture process, typically omitted in translocation simulations, is essential to translocation modelling. As the standard error scales like $\sim 1/\sqrt{N}$, there are diminishing returns with increasing N . It is not necessary to use longer lengths and those used here prove sufficient. In addition, as simulating the capture process is computationally expensive, there are limitations in the number of runs that can be performed. Although scaling trends can be recovered in as few as 300 runs, a minimum of 1000 runs for each distinct simulation condition is necessary to confidently reflect the statistical variance in the data. Thus, reviewing at least 2000 independent simulation runs for each condition provides an appropriate balance between computational expense and accuracy.

Chapter 5

RESULTS

5.1 Review of Results

For both the standard and capture protocols (see Ch. 4), conformational changes in polymer chains of length $N = 50, 100, 200$ were recorded during the translocation process. By examining the compression and elongation of a polymer via its radius of gyration it was possible to comment on the shortcomings of current simulation methodologies and offer a possible explanation for the discrepancies often found between experiment and simulation.

5.1.1 Simulation Cases

Before reviewing the results, it may be of benefit to first restate the defining characteristics of the simulation methodologies used. Recall that there are two simulation protocols; the standard protocol, in which the polymer begins translocation pre-threaded in the nanopore, and the capture protocol, in which the polymer first diffuses towards the nanopore before threading for translocation. Note that in the standard protocol the electric field is applied only within the nanopore and in the capture protocol the electric field extends outward from the nanopore to model the nanopore pulling in on its *cis* side and pushing

out on its *trans* side. In addition, both of these protocols are run at two different Péclet values to quantify the drift-diffusion balance; a default Péclet value which is typically used as a default setting in current simulation literature, and a tuned Péclet value which reflects prior work that tuned the drift-diffusion balance of simulations to more closely match experimental conditions. Thus, there are four independent cases: standard-default (SD), standard-tuned (ST), capture-default (CD) and capture-tuned (CT).

5.1.2 Event Types

Table 5.1 summarizes the number of runs performed at each Péclet value for the capture protocol. Although 2000 *successful* translocation events were recorded for each N , the possibility exists for a simulation to instead be terminated via a stuck or diffused away event (ref. Sec. 4.2.2), thereby increasing the overall number of simulations performed under either Péclet condition. Counts of the standard protocol are not included as the polymer either completes translocation or fails. For consistency, 2000 standard translocation events are also recorded for each N .

Recall that stuck events are those in which the polymer is compressed against the membrane at the mouth of the nanopore for an extended period of time unable to overcome the energy barrier to thread by an end. Diffused away events are those in which the polymer initially diffuses away from the nanopore and passes beyond the cutoff distance.

When comparing across N , stuck events are more likely under tuned P conditions where the polymer approaches the nanopore in an elongated configuration. Here diffusion is suppressed; a polymer that does not thread quickly will

TABLE 5.1: Counts of Capture Protocol Event Outcomes

<i>P</i> value	Polymer Length	Stuck	Diffused Away	Translocated
Default Péclet	50	1171	475	2000
	100	511	377	2000
	200	267	287	2000
Tuned Péclet	50	1081	1836	2000
	100	1404	1751	2000
	200	1750	1250	2000

become stuck, unable to relax or produce large enough thermal kicks to reorient and attempt to thread by an end. Under default P conditions however, the opposite is true and a polymer which may at first appear to be stuck can more readily reorient itself and thread by an end.

The number of diffused away events decreases as N increases for both Péclet numbers. For longer polymers, diffusion is a reduced effect and this is reflected in the simulation where more polymers are captured by the nanopore than diffuse away. However, when a polymer is captured it may either translocate successfully or become stuck. The additional thermal energy available under default P permits a greater number of potentially stuck polymers to instead thread for successful translocation.

5.2 Polymer Configurations

5.2.1 Standard Protocol

Fig. 5.1 shows both the parallel (on-axis with nanopore), $R_{g\parallel}$, and perpendicular, $R_{g\perp}$, radius of gyration for the standard protocol translocation results. For all N , $R_{g\parallel}$ and $R_{g\perp}$ are recorded at the start of translocation and again after

translocation once the polymer has fully passed through the nanopore. These values are compared against the equilibrium radius of gyration, $R_{g_{eq}}$, denoted by the dashed horizontal line in Fig. 5.1, for both default and tuned Péclet numbers. It is important to point out that the error bars in Fig. 5.1 represent the standard deviation of the average polymer configuration found at each stage, and therefore represent the variability in R_g , thus identifying the likelihood the polymer will be found in a compressed or extended state at either stage of the translocation process. Note that the standard error is on the order of the data points and reflects confidence in the mean R_g reported for each stage.

Default Péclet

At default P the polymer is found in a near fully equilibrated conformation at the start of translocation. There is slight extension of the polymer on-axis and $R_{g_{||}}$ increases only slightly with increasing N . $R_{g_{\perp}}$ however, shows small increases in compression as N is increased. Here the slight distortion reflects the standard protocol's initial condition of prethreading the polymer for translocation—there is a natural repulsion of the polymer away from the membrane. However, as this distortion is minimal, the polymer is considered to be in an equilibrium conformation.

After translocation the polymer is compressed in both parallel and perpendicular directions. The compression of both $R_{g_{||}}$ and $R_{g_{\perp}}$ below $R_{g_{eq}}$ occurs for all N and in fact this compression increases with increasing N . This is a direct result of crowding effects on the *trans* side of the nanopore as there is no external field to pull the monomers away from the nanopore. With the field applied only on the inside of the nanopore, each consecutive monomer exiting on the *trans* side leads to an increase in monomer density and smaller R_g values. This

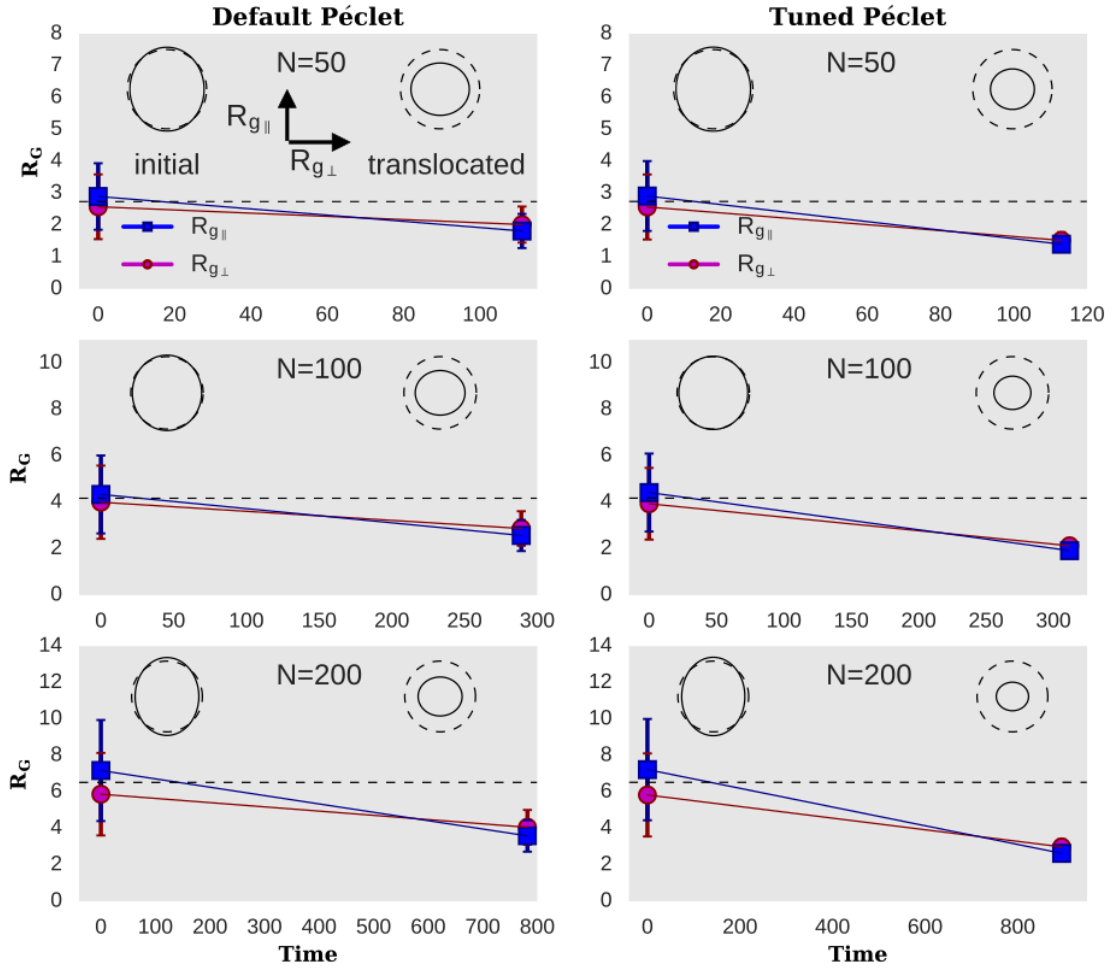


FIGURE 5.1: Results of the standard protocol at both Péclet values. The y-axis indicates the average radius of gyration, R_g , and the x-axis the average time. Here $t = 0$ corresponds to the release of the polymer and start of translocation. Both $R_{g,\parallel}$ and $R_{g,\perp}$ are compared at both stages with the dashed horizontal line referencing the equilibrium conformation of the polymer. Error bars indicate the variation in R_g observed and as such refer to the standard deviation not the confidence in the data points; the standard error is on the order of the data points themselves. The dotted ellipses correspond to the equilibrium conformation of the polymer with solid superimposed ellipses representative of the average configuration of the polymer at each stage. All ellipses are drawn to scale.

effect grows as the number of monomers increase, and so, for longer polymers the compression is more pronounced.

Tuned Péclet

At tuned P the polymer is also found in a near fully equilibrated conformation at the start of translocation. Post-translocation the polymer is compressed below $R_{g_{eq}}$ in both $R_{g_{||}}$ and $R_{g_{\perp}}$. However, due to suppressed diffusion effects under tuned P conditions the compression is greater than in default P , and this can be explained by the decrease in thermal energy available to the polymer for relaxation through random kicks. Instead of slowly dispersing away from the nanopore exit, the monomers remain closer longer, increasing in density and thus crowding effects are more pronounced, with R_g increasingly falling below $R_{g_{eq}}$ at longer N .

5.2.2 Capture Protocol

Fig. 5.2 shows both the parallel, $R_{g_{||}}$, and perpendicular, $R_{g_{\perp}}$, radius of gyration for the capture protocol translocation results. For all N , $R_{g_{||}}$ and $R_{g_{\perp}}$ are recorded at each of the five stages of the capture protocol: transport, contact, first thread, last thread and translocation. These values are compared against the equilibrium radius of gyration, $R_{g_{eq}}$, denoted by the dashed horizontal line in Fig. 5.2, for both default and tuned Péclet numbers. Since the transport stage of the capture protocol is simply the fully equilibrated polymer transported closer to the nanopore this stage is not shown in Fig. 5.2, and is instead reflected by the dashed horizontal $R_{g_{eq}}$ line. Additionally, the x-axis is shifted such that

time $t = 0$ now coincides with the contact stage and where the average duration of all successive stages are thus described relative to making contact at time $t = 0$.

As with the standard protocol results, the error bars in Fig. 5.2 represent the standard deviation in the configurations and so reflect the variability in R_g . Thus, for all stages of the capture protocol, the variability of the polymer existing in a compressed or elongated configuration is provided. As before, the standard error is on the order of the size of the data points and therefore reflects small uncertainty in the mean values reported.

Equilibration & Transport: (not shown in Fig. 5.2) After the polymer is first relaxed in free space, $R_{g_{||}}$ and $R_{g_{\perp}}$ are found to be in agreement with $R_{g_{eq}}$ and this holds true for all polymer lengths simulated under both Péclet conditions. While keeping the equilibrated configuration intact, the polymer is then transported closer to the nanopore in preparation for the start of the simulated capture process. In Fig. 5.2, $R_{g_{eq}}$ of the equilibrated polymer is denoted by a dashed horizontal line for both P values. Additionally, Fig. 5.3 highlights the nonequilibrium shapes the polymer progresses through during the capture process with $R_{g_{eq}}$ provided as a dotted ellipse for reference.

Default Péclet

At default P the polymer is generally found below $R_{g_{eq}}$ and stretched slightly on-axis. As N increases, the duration between first and last thread dominates the time scale and this is reflected in the increased compression in both $R_{g_{||}}$ and $R_{g_{\perp}}$ for longer N .

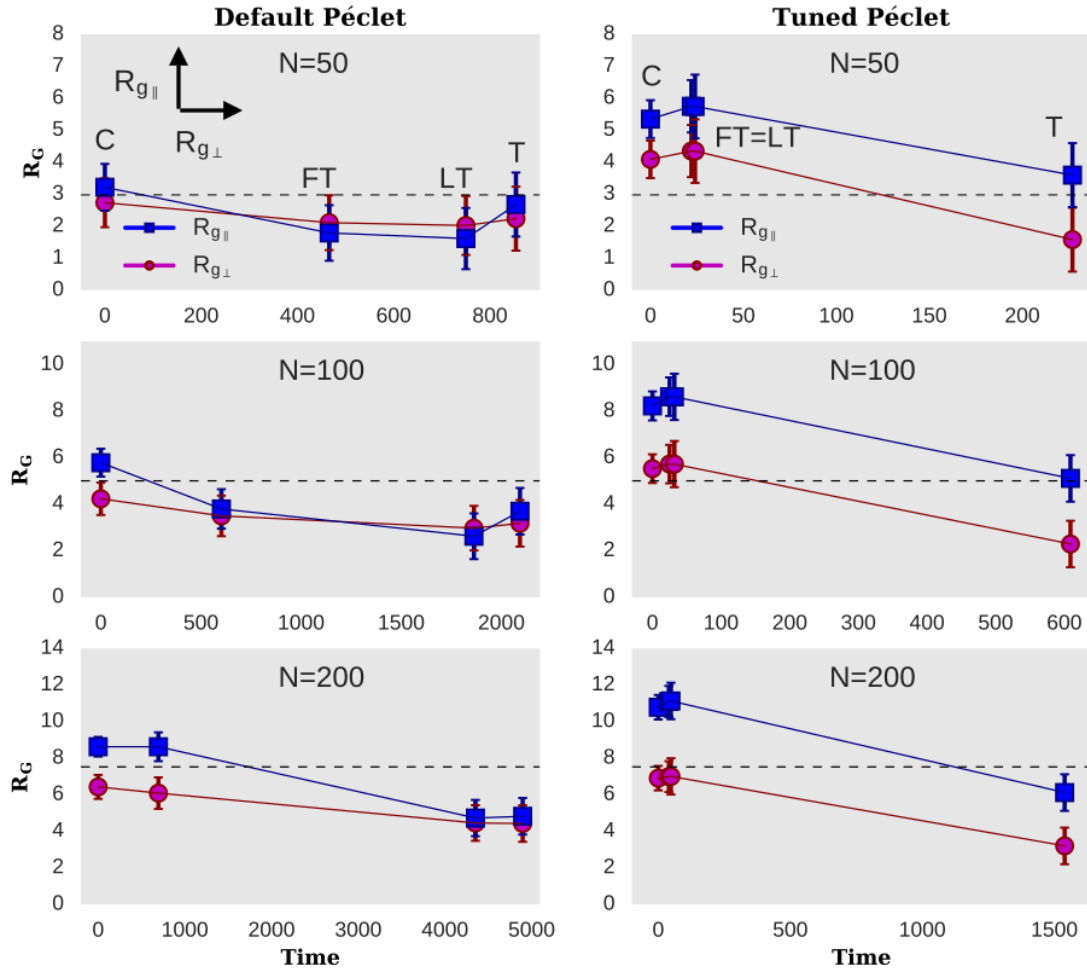


FIGURE 5.2: Results of the capture protocol at both Péclet values. The y-axis indicates the average radius of gyration, R_g , and the x-axis the average time. Here the four phases of the capture protocol: contact **C**, first thread **FT**, last thread **LT** and translocation **T**, are identified. Both $R_{g_{||}}$ and $R_{g_{\perp}}$ are compared at both stages with the dashed horizontal line referencing the equilibrium conformation of the polymer. Error bars indicate the variation in R_g observed and as such refer to the standard deviation not the confidence in the data points; the standard error is on the order of the data points themselves. Please refer to Fig. 5.3 for detailed schematics of polymer configurations.

Contact: When the polymer first makes contact with the nanopore there is a slight elongation in $R_{g\parallel}$. This stretching is a result of the monomers being driven in towards the nanopore as the polymer passes into regions of high field strength. Due to gradients near the mouth of the nanopore, monomers approaching this region first will experience a stronger force than those monomers farther away, thus creating an unbalanced rate of transport that extends the polymer. As N is increased, $R_{g\parallel}$ rises further above the $R_{g_{eq}}$ line and Fig. 5.2 illustrates how the external field counters diffusion by pulling the polymer out of a relaxed conformation. Accordingly, the polymer also experiences compression in $R_{g\perp}$ proportionate to the amount it is stretched on-axis and, when the polymer length is increased, $R_{g\perp}$ drops further below $R_{g_{eq}}$. Fig. 5.4 identifies which monomer is most likely to make contact with the nanopore first. Although there are more individual events for on-end contact, the majority of contact events for default P occur from monomers elsewhere along the polymer chain.

First Thread: As the nanopore's diameter is only wide enough for one monomer, it forces single-file translocation of polymer. Although the polymer must thread for translocation, Fig. 5.4 also reveals a fair number of contact events where the polymer arrives by a more central monomer. Indeed, regardless of which monomer initially makes contact, translocation is still likely to occur, and is largely attributed to the highly diffusive environment; the polymer is continuously reorienting via thermal kicks such that an end monomer will eventually locate the nanopore and thread. It is this variability in time, the duration from contact through to a successful thread, that defines the characteristics of the

capture protocol at default P . Fig. 5.5 provides distributions of the threading time for all events that end in translocation (as opposed to stuck or diffused away).

For default P the threading time can become quite lengthy and directly reflects the time spent by the polymer fluctuating at the nanopore waiting for an end to thread. In fact, this process may last long enough for the external field to push the polymer such that it crowds the *cis* side of the nanopore.

In Fig. 5.2, first thread is shown compressed in both $R_{g\parallel}$ and $R_{g\perp}$ directions for $N = 50$ and $N = 100$, with both values below $R_{g_{eq}}$. $N = 200$ finds compression in $R_{g\perp}$ below $R_{g_{eq}}$ while $R_{g\parallel}$, although slightly compressed from contact, remains above $R_{g_{eq}}$. This reflects the increase in N where it is likely for a thread event to occur on one end of the polymer while the rest has not yet been compressed closer. For all N at default P , the average polymer configuration transitions from slightly elongated at contact to slightly compressed at first thread. Fig. 5.3 depicts schematics of the polymer configurations as they relate to Fig. 5.2.

Last Thread: The last thread stage of the capture protocol can be compared to the initial stage of the standard protocol: Recall the polymer is equilibrated with an end prethreaded, and both the initial and last thread stages directly precede translocation. As diffusion is favoured under default P , there is sufficient energy available for thermal kicks to jostle the polymer such that it retracts from the nanopore after it threads. In the standard protocol the simulation would be terminated as there is no external field profile to guide the polymer back to the nanopore. The capture protocol however, facilitates rethreading of the polymer and this can in fact happen many times. If the polymer was not already

compressed during the first thread attempt (such as first thread at $N = 200$ in Fig. 5.2), the increased time spent fluctuating, retracting and rethreading, will undoubtedly position the polymer to incur additional field effects, driving it further into a compressed state for both $R_{g\parallel}$ and $R_{g\perp}$ directions.

Fig. 5.2 verifies this compression for all N ; particularly for $N = 200$ where $R_{g\parallel}$ crosses over from an extended conformation above $R_{g_{eq}}$, and joins $R_{g\perp}$ in a compressed state below $R_{g_{eq}}$. The polymer configurations at $N = 50, 100$ were already compressed to the point that no significant change was observed. Comparisons of the polymer conformations at all stages are compared against $R_{g_{eq}}$ in Fig. 5.3.

Translocation: On the *cis* side of the nanopore, the external field is responsible for the ongoing compression of the polymer in both $R_{g\parallel}$ and $R_{g\perp}$ directions just prior to translocation. With each of the polymer's N monomers particularly close to the mouth of the nanopore, the final stage of the translocation process is able to finish quite fast. As the capture protocol was designed with a full external field profile, the field begins on the *cis* side, flows in through the nanopore and fans upward and outward on the *trans* side of the nanopore (re: Fig. 4.2). Therefore, as each monomer exits on the *trans* side during translocation, the field continues to drive the monomers up and away from the nanopore's exit. This is fundamentally different than the results reported via the standard protocol. With no external field, the monomers in the standard protocol exhibit crowding by the *trans* exit of the nanopore. Here, at default P , both $R_{g\parallel}$ and $R_{g\perp}$, for all N , are elongated compared to the more compressed conformation the polymers displayed at last thread. The schematics in Fig. 5.3 illustrate how

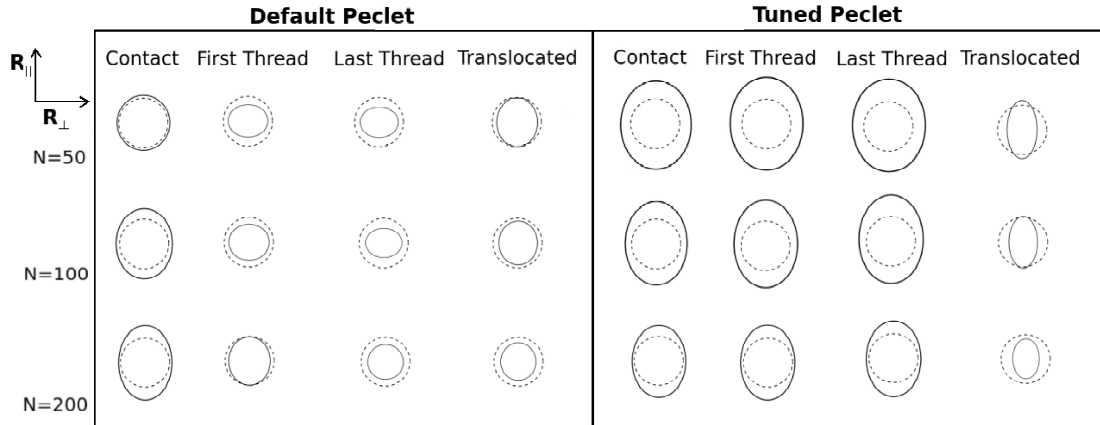


FIGURE 5.3: Polymer configurations for the capture protocol at both Péclet numbers. Solid ellipses represent the average polymer conformation at each stage with dotted ellipses referencing the equilibrium configuration of the polymer. Ellipses are scaled to $N=50$ equilibrium.

results from the capture protocol deviate from the crowded, compressed polymer configurations of the standard protocol post-translocation.

Tuned Péclet

At tuned P there is an even greater difference in polymer conformations at all stages of the capture process than was found with either Péclet value in the standard protocol or under default P conditions in the capture protocol. Fig. 5.2 clearly illustrates a bias towards an extended polymer conformation regardless of the capture-process stage: elongated along $R_{g||}$ and compressed along $R_{g\perp}$. Here, all but the final translocated stage appear to exhibit both $R_{g||}$ and $R_{g\perp}$ greater than $R_{g_{eq}}$. In contrast to default P , where the threading process dominates the time scale, here, under tuned P conditions, the duration of the translocation stage is most prominent.

Contact: At tuned P , when a polymer makes contact with the nanopore the

elongation along $R_{g_{||}}$ is substantially more pronounced for all N than it is under default P conditions. By suppressing diffusion, the polymer's ability to relax is affected, and, as a result, the polymer is unable to counter the extension caused by the field gradients driving each successive monomer towards the nanopore. Furthermore, a significant difference between Péclet values is found in $R_{g_{\perp}}$. For lower N at tuned P , $R_{g_{\perp}}$ is well above $R_{g_{eq}}$, but this extension decreases for longer polymers, where, at $N = 200$, $R_{g_{\perp}}$ drops just below $R_{g_{eq}}$ causing instead a slight compression of the polymer orthogonal to the pore axis. As the polymer is pulled in towards the nanopore it is uncoiled and elongated by an end (or near-end) with shorter polymers becoming nearly completely uncoiled by the time a monomer makes contact. Longer polymers, when extended by an end, will most likely make contact while the majority of their monomers remain coiled, not yet pulled by the external field. Additionally, as the polymer can approach the nanopore from all angles of a *cis* side hemisphere, shorter polymers that are approaching from directions where they are aligned more parallel to the membrane will appear to have full extension in $R_{g_{\perp}}$ and full compression in $R_{g_{||}}$, balancing the extension expected in $R_{g_{||}}$ from the field. This effect lessens as polymer length increases as the extended portion contains less monomers and the bulk of the polymer, regardless of approach angle, remains coiled as it was before being pulled by the field. Thus, for longer N , the average conformation in $R_{g_{\perp}}$ remains similar to its shape prior to contact.

First Thread: Referring back to Fig. 5.4, contact events recorded at tuned P identify that successful translocation events occur for nearly all polymers that arrive at the nanopore by an end (or near-end) monomer. When compared to default P , the effect of suppressing diffusion necessarily also suppresses the

polymers ability to reorient or relax with time. Thus, the majority of contact events where the polymer arrives by a more centrally located monomer are terminated as stuck events. Table 5.1 confirms that for all N at tuned P , there are at least half as many stuck events for the translocated events. Thus a condition naturally emerges whereby successful polymer configurations at tuned P require that initial contact with the nanopore be on-end. When this pre-oriented configuration crosses into the field gradients, an end (or near-end) monomer is always captured first and, as it is driven towards the nanopore, pulls the rest of the polymer along. Without sufficient diffusion the polymer cannot relax and so is forcibly extended by the front end.

For all N , both $R_{g_{||}}$ and $R_{g_{\perp}}$ are extended into configurations more elongated than they were at contact. These extended conformations promote threading by an end and therefore the first thread occurs very soon after contact, substantially reducing the overall threading time. The significance of tuned P threading times is seen in Fig. 5.5 where, in stark contrast to default P , almost every event is clustered at incredibly short thread times with only very few events at longer times. Looking to Fig. 5.2 and Fig. 5.3 the effect the Péclet number has on the capture process is quite clear. At default P and across N , the polymer is typically compressed below $R_{g_{eq}}$ in both $R_{g_{||}}$ and $R_{g_{\perp}}$ directions. At tuned P the opposite is true- across N , the polymer is typically elongated above $R_{g_{eq}}$ in both $R_{g_{||}}$ and $R_{g_{\perp}}$ directions.

Last Thread: For the capture protocol at tuned P , the first thread event is quite often also the last thread event. This is a direct result of both the polymer initially threading very fast and, with suppressed diffusion, the polymer is highly

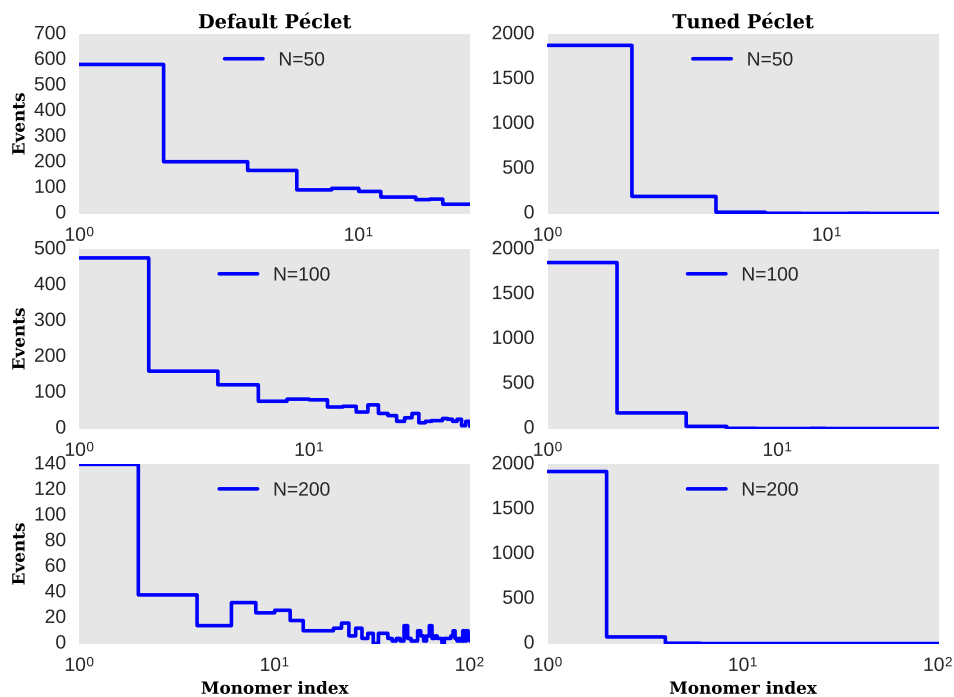


FIGURE 5.4: The first monomer to make contact with the nanopore was recorded for each successful translocation. Here the index of the monomer is shown in log-scale on the x-axis and the symmetry of the polymer is used such that the index extends from 0 to $N/2$ where N is the polymer length. For both Péclet cases rapid decay is observed as the monomer index moves away from either end.

unlikely to retract back to the *cis* side after threading. Thus the polymer remains elongated and in Fig. 5.2, for all N , last thread is nearly indistinguishable from first thread.

As mentioned, last thread of the capture protocol most resembles the initial stage of the standard protocol. Recall that under both Péclet values the standard protocol begins translocation in a nearly uniform, relaxed equilibrated conformation. Referring to both Fig. 5.1 and Fig. 5.2, and the schematics in Fig. 5.3, it is clear that the assumption of a polymer in a relaxed equilibrated state just prior to translocation is qualitatively erroneous. In contrast to the standard protocol,

results of the capture process at default P indicate a polymer would instead be found in a compressed conformation prior to translocation. Likewise, for tuned P , the polymer is very clearly elongated for most of the capture process, including thread events prior to translocation.

Translocation: On the *cis* side of the nanopore, under tuned P conditions, the polymer is typically elongated just prior to translocation. As the polymer passes through the nanopore, it will slowly transition from an elongated configuration to one that is more compressed. With lower diffusion the monomers rely almost exclusively on the external field to propel them up and away from the *trans* side exit. As each monomer exits the nanopore, it is caught by the external field, and, similar to contact and first thread, is driven away from the nanopore. This time however, the monomers travel fastest when they first leave the pore and slow down as the field drops off. With lower diffusion the monomers accumulate where the field drops off, pushed outward and upward now only by the outgoing monomers still being driven by the field.

For all N , the translocation process compresses $R_{g\perp}$ far below $R_{g_{eq}}$, but the drift dynamics on the *trans* side assist in extending $R_{g\parallel}$ (as compared to $R_{g\perp}$). As N is increased however, the rate of extension slows on the *trans* side as the more recent monomers being driven out of the nanopore are blocked from moving upwards by previously translocated monomers and instead are pushed into emptier regions off-axis. Thus, $R_{g\parallel}$ at tuned P decreases as N increases until it is below $R_{g_{eq}}$ for $N = 200$.

When shown side-by-side (compare Fig. 5.1-Fig. 5.3), the sharp contrast between results obtained through the standard protocol and those with the capture protocol are clear. By implementing the extended translocation process,

the capture protocol recovers polymer behaviour that appears to more closely match general experiment conditions. The standard protocol, on both Péclet accounts, fails to replicate proper polymer conformations for both the pre- and post-translocation stages.

5.3 Time Scales

Apart from illustrating qualitative differences in the polymer configurations (ref. Sec. 5.2), the capture protocol also reveals interesting quantitative changes in the translocation dynamics. Referring once again to Fig. 5.2, it is evident that the time scales between phases of the protocol change, both as N is increased, and between P values. Specifically, the highly visible differences in threading time reveal fundamental changes in the system between P numbers. Fig. 5.5 provides the thread times from successful translocation events for each N . Here, the impact of changing the P number is magnified with the use of a semi-log scale in y . As the standard protocol does not simulate any phase prior to translocation, there are no dynamical changes over N or between P values; the only time scale, the translocation time, is discussed in Sec. 5.4.

Recall that the thread time is defined as the total duration from when the polymer first makes contact with the nanopore up until it begins translocation (stages 'contact' through to 'last thread' of the capture protocol). Note that this necessarily includes all additional thread attempts that may occur between first and last thread.

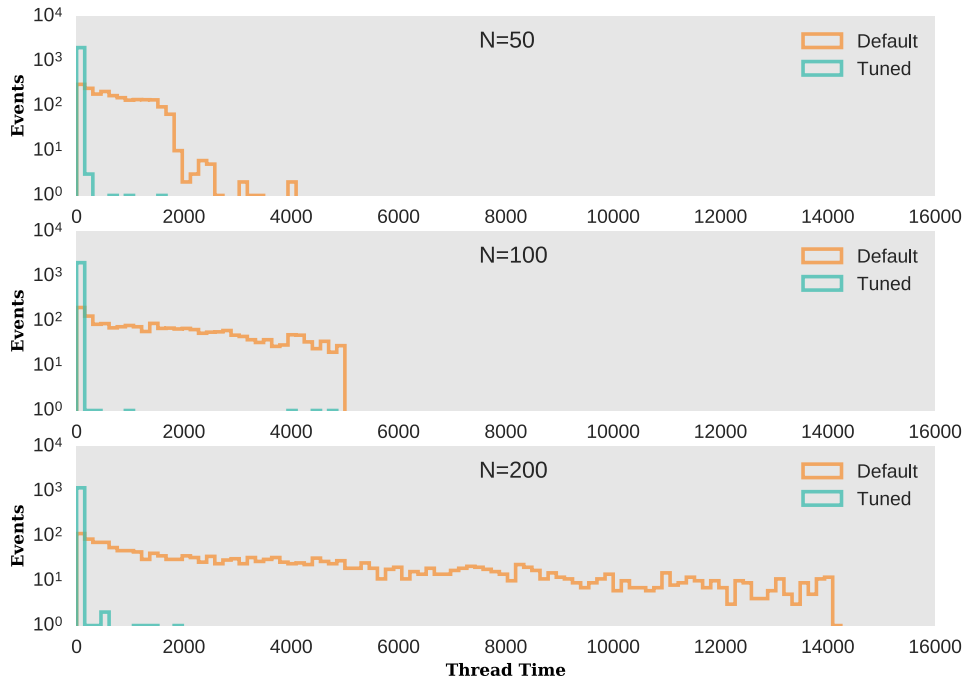


FIGURE 5.5: The distribution of threading times for both Péclet values in the capture protocol. Here a logarithmic scale in y (the number of events) illustrates the exponential decay in thread times per event for default P . In stark contrast, at tuned P , the majority of all successful translocation events are preceded by very short thread times.

5.3.1 Default Péclet

At default P the system is dominated by diffusion, which, as seen in Sec. 5.2, permits continuous relaxation of the polymer. As a result, regardless of N , the polymer is significantly more likely to be found in a more compressed conformation along all phases of the capture-translocation process. During threading, there is competition between the random thermal fluctuations and the external force driving the polymer towards the nanopore and this prevents the polymer from quickly moving from contact and threading to translocation. In Fig. 5.2

it is clear that the overall thread time increases with increasing N . Lengthening the polymer increases this competition between the two forces as there are more monomers available to get 'caught' by the external field. The external field is likened to the suppression of random movement whereas thermal fluctuations define random movement. Thus, the bottle-neck to translocation at default P is threading itself. The constant competition of being driven towards, then stuck and compressed against the membrane while also being repulsed by the membrane, creates a dynamic situation that prevents an end monomer from quickly locating the mouth of the nanopore. As N increases, there are even more monomers competing to thread and this is reflected in the longer thread times.

Similarly, the balance of time duration between contact to first thread and first thread to last thread is also affected. With only $2/N$ monomers available to thread (leading to successful translocation), it is clear that as N increases, the time it takes for an end to thread is the dominate contribution to the threading bottle-neck. In fact for all N , the duration between contact to first thread remains about the same but the duration between first thread and last thread increases by a factor of ~ 4 .

Fig. 5.5 shows the exponential decay (linear on the semi-log plot) of threading times for default P . Due to the inherent traits of randomness, here exhibited by the thermal fluctuations, there is a large variance in the thread times that have preceded a successful translocation. With no favoured configuration or orientation of the polymer, it is possible for an end monomer to thread once, twice, ten times or more. However, once full threading occurs the actual translocation of the polymer through the nanopore happens relatively quickly.

Fig. 5.7 and Fig. 5.8 are snapshots from simulations of polymers threading under default P conditions. Similar to Fig. 5.4, Fig. 5.6 also illustrates the distribution of monomer indexes that first make contact with the nanopore. In addition, the distribution in monomer index of the first monomer(s) to achieve first and last thread is also presented. For both Péclet cases rapid decay is observed as the monomer index moves away from either end for all stages. However, under tuned P conditions, the more likely on-end contact of the polymer clearly facilitates fast threading with first thread occurring by an end monomer which almost always also becomes the last thread. Under default P , the progression towards on-end translocation from the more likely central monomers making contact is quite evident.

5.3.2 Tuned Péclet

In contrast, Fig. 5.5 emphasizes how the thread times for tuned P are clustered at significantly much shorter durations. With diffusion suppressed, the polymer is more likely to arrive at the nanopore in an elongated state (parallel to the local external field). Thus the polymer is considerably more favourably oriented for threading by an end. With no significant time spent threading, retracting and rethreading while waiting for an end monomer to thread, those events in which translocation is successful are preceded by very quick thread times. Note that at tuned P there is an increase in the possibility of stuck events arising from the diminished thermal fluctuations of the polymer which prevent reorientation (relaxation). As such, the system effectively omits all events save for those which are successful, and therefore thread relatively quickly. This is also reflected in Fig. 5.2 where, at all N , the first thread is often the only thread,

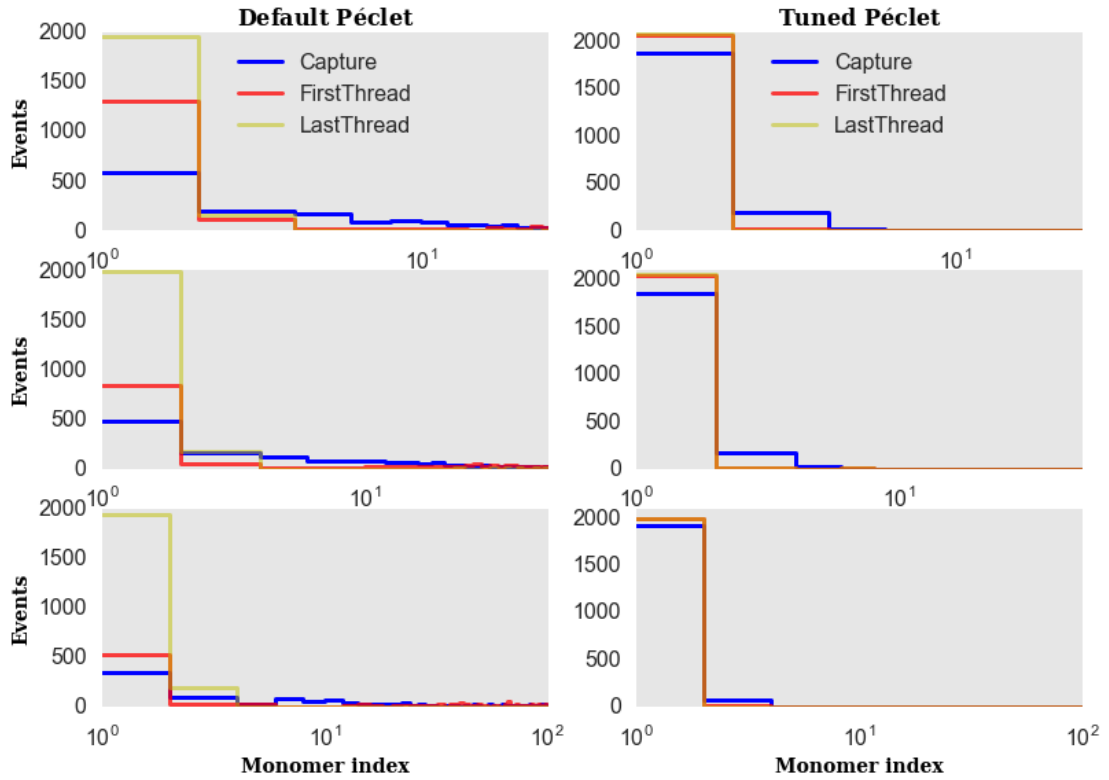


FIGURE 5.6: The first monomer to make contact, first thread and last thread with the nanopore was recorded for each successful translocation. Here the index of the monomer is shown in log-scale on the x-axis and the symmetry of the polymer is used such that the index extends from 0 to $N/2$ where N is the polymer length.

and therefore also the last thread; the result of which cuts the duration of the threading process down significantly.

Overall, the duration of the threading process at tuned P is ~ 30 times lower than at default P . It is interesting to note that the same effects that permit a faster thread time at tuned P are also responsible for significantly extending the duration of the translocation phase. By arriving extended in a diffusion limited environment, the polymer exhibits tension along its length as it is driven towards the nanopore. With no substantial thermal diffusion to help push the

polymer together, each monomer is essentially 'caught' by the field one-by-one. Thus those monomers near the 'front' of the polymer begin to move at a different rate than those closer to the rear. As a result, tension is propagated through the chain. With the force of the external field increasing closer to the nanopore, the force felt by each monomer along the extended chain is considerably different from one end to the other. Each monomer must effectively 'pull' those directly behind it. It is not difficult to imagine how, in this situation, a drag force emerges, slowing the movement of the polymer as a whole. As N increases, this 'drag' necessarily increases slowing the translocation portion of the capture process down considerably, particularly when compared to translocation times at default P . Fig. 5.9 is a simulation snapshot of a polymer threading under tuned P .

5.3.3 Escape Process

The linear relationship shown in Fig. 5.5 implies that the threading times obey an exponential decay when in default P conditions. This is characteristic of a Kramers escape process which describes how a polymer can escape from a potential well due to a random walk from thermal fluctuations [50]. Here the polymer is being compressed strongly and consistently against the membrane over time due to the external forces pushing the polymer along the field lines and into the pore. Thus, during the threading process an energy cost will emerge if the polymer is unable to thread quickly. Eventually, as compression increases over time, the energy cost to the polymer to thread by an end becomes quite significant. This is because the polymer must overcome an effective energy barrier ($E \gg k_B T$) by diffusing backwards against the field gradient. The only way the polymer can overcome this energy barrier is with a large enough thermal

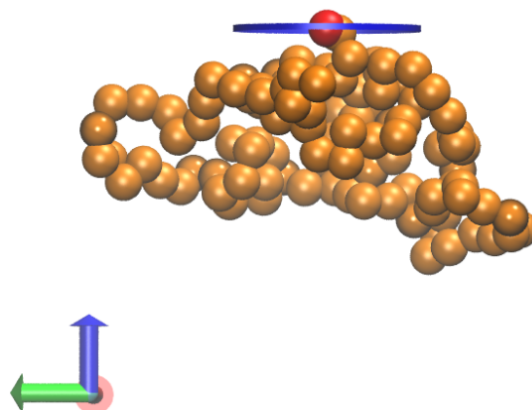


FIGURE 5.7: A typical conformation for polymers threading under default P . Here $N = 100$. Compression along $R_{g||}$ is increased as the polymer waits for an end to thread.

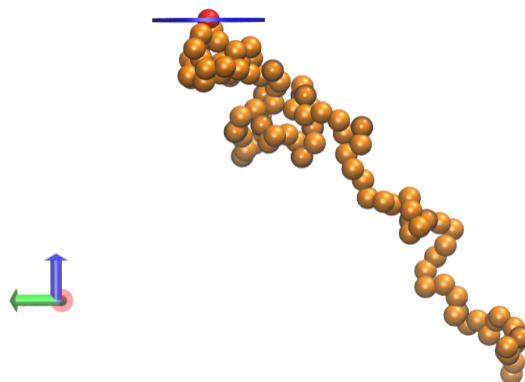


FIGURE 5.8: An atypical conformation for polymers threading under default P . Here $N = 100$ and represents the same stage of the capture-translocation process as in Fig. 5.7. Although elongated, the on-end extension associated with tuned P results is absent (see Fig. 5.9).

kick to disrupt the compression, creating the possibility for an end to come free and find the pore entrance. If the polymer is unable to do this, it will tend to remain trapped and trigger a stuck event.

Under tuned P conditions, due to the polymer almost always arriving on end for contact, it is highly unlikely for the polymer to get stuck waiting to

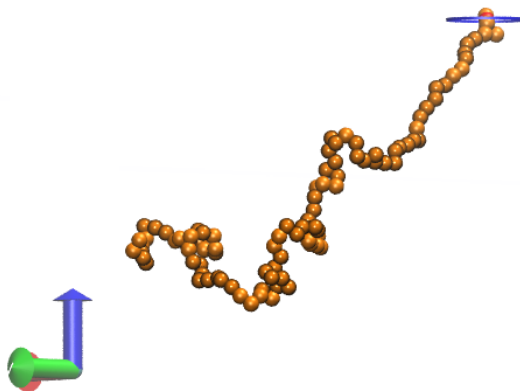


FIGURE 5.9: A typical conformation for polymers threading under tuned P . Here $N = 100$. Notice the on-end elongation of the polymer extending towards the nanopore. There is a clear transition along the chain where monomers in tension with adjacent monomers emerge as the field pulls them towards the nanopore.

thread. However, although unlikely, even under these conditions the polymer can occasionally approach the nanopore in a configuration unfavourable for threading thus becoming trapped. Here, the suppression of diffusion results in insufficient thermal energy available for the polymer to produce a large enough kick to reorient itself for threading. These stuck events are therefore terminated, unlike under default P conditions, where the likelihood of a large thermal kick occurring is substantially increased, permitting successful threading.

5.4 Distribution of τ

Undoubtedly, one might expect the translocation time, τ , to feature prominently in polymer translocation research. This core characteristic of the process is used as the basis for polymer scaling laws and here, permits an enlightening revelation of the sensitivity of current computational models. In Fig. 5.10 the translocation times from all successful events are presented as distributions

for each protocol and Péclet value. It is immediately clear that the inclusion of the capture process in the simulation model has a dramatic effect on τ and this divergence grows as N is increased.

The distributions of the standard protocol results are quite normally distributed; the Gaussian-like behaviour is preserved at both Péclet numbers with longer mean translocation times reflecting an increase in N . By comparison, the capture protocol exhibits a tendency towards positive skewness under default Péclet conditions and negative skewness under tuned Péclet conditions with both capture protocol distributions having mean τ values distinct from those obtained via the standard protocol. Incidentally, these results suggest the possibility of engineering nano-devices that take advantage of this difference in τ by controlling the specific drift-diffusion balance of a system.

In addition, Fig. 5.11-5.13 provide scatter plots of the translocation time of all 2000 events successfully completed for all protocols. Each figure represents data for each of the $N = 50, 100, 200$ polymers. Here τ is compared to R_g of the polymer. As N is increased, the most prominent feature is the clustering of data in the standard protocol under default P . Here the long tail in the distribution described in Fig. 5.10 is evident. At $N = 200$ the high concentration of small R_g and fast τ directly illustrates how the compression of a polymer prior to translocation reduces τ significantly.

Also visible is the substantial shift to longer τ for the capture process at tuned P (bottom-right inset in Fig. 5.11-5.13). While the standard protocol at both P and (to some extent) the capture protocol at default P produce translocation events on similar time scales, the translocation times for the capture protocol at tuned P are ~ 2 times longer. This once again reflects how a nonequilibrium conformation- in this case elongation, has a substantial effect on the

results obtained.

5.4.1 Standard Protocol

The similarities of the standard protocol distributions are predictable. With the polymer reaching equilibration while an end is fixed inside the nanopore, both Péclet values will see the polymer begin translocation with its monomers relatively close to the mouth of the nanopore, limiting drag effects. Even with diffusion suppressed, as in the tuned Péclet state, the remaining monomers are able to reach the mouth of the nanopore relatively quickly due to their close proximity. The top panel in Fig. 5.11-5.13 illustrates the symmetry between R_g and τ . In both P cases, Fig. 5.10 shows how the mean increases with N and this is attributed to the increase in the amount of monomers passing single-file through the nanopore. However, as N increases, it is clear that the mean grows (slightly) faster at tuned P . Here, as more monomers are added to the polymer chain, the average distance to the nanopore for the monomers increases. With diffusion suppressed and no external field, there is no additional assistance to help move the monomers faster in towards the nanopore, and so τ is increased. However, under default P there is the chance for a thermal kick to help push the monomers in towards the nanopore and this assists in decreasing the translocation time.

5.4.2 Capture Protocol

Default Péclet

By simulating the capture of the polymer prior to translocation a number of features have emerged. At default P the polymer is able to relax and this is true

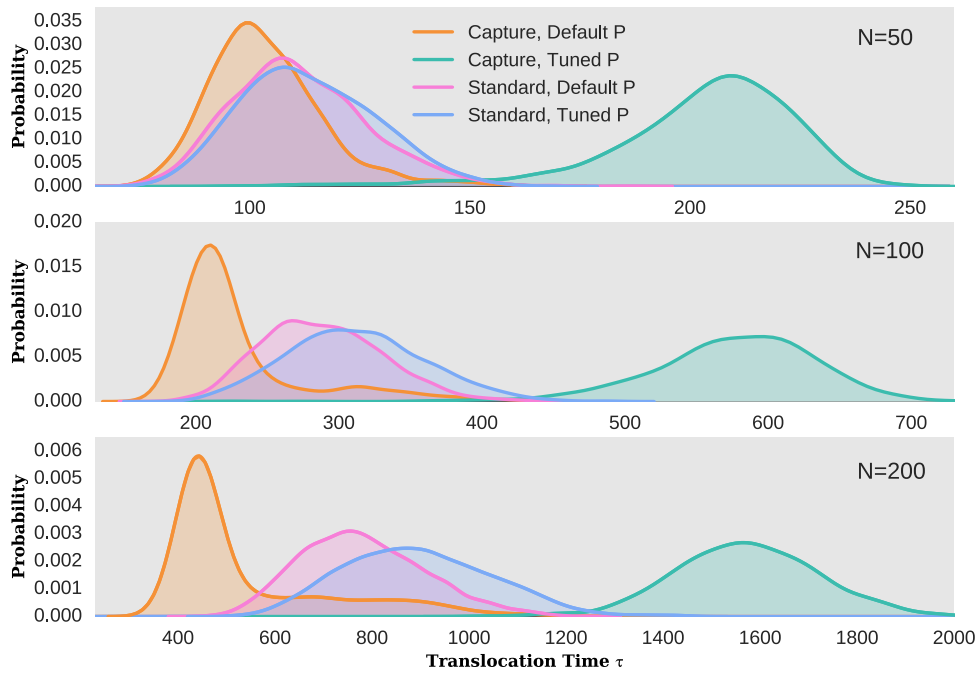


FIGURE 5.10: The distribution of translocation times for both Pécel values of the capture and standard protocols are overlaid for polymer lengths of $N = 50, 100, 200$.

even in high-field regions close to the nanopore. However, although more likely to be closely packed, a more elongated polymer conformation may occur (ref Fig. 5.8). Thus, although there is an identifiable peak in τ at short times, a long tail emerges reflecting those occasional events with longer translocation times. Here, as described earlier, the more stretched a polymer is prior to translocation the more drag there is to slow the process.

In Fig. 5.5 threading times for default P are widely dispersed from short thread times to considerably longer thread times. When a polymer is unable to thread by an end quickly, the external field will eventually push the polymer in towards the membrane and into a compressed configuration. For successful

translocation events preceded by a polymer in a compressed state, fast translocation times are obtained. Thus the large number of events with long thread times, as shown in Fig. 5.5, result in events with short translocation times found in the main peak of the capture-default (CD) distribution in Fig. 5.10. Likewise, the thread events in which an end monomer threads relatively quickly, as represented by the exponential decay in Fig. 5.5, are associated with more elongated polymers and contribute to the translocation events with longer τ found in the extended tail of the distribution. The bottom-left inset of Fig. 5.11-5.13 identifies the emergence of a strong peak clustered around low R_g values as N is increased. Here, the emphasis of fast translocation times is clear for compressed polymers.

Since a direct result of the highly diffusive environment is an increase in the random fluctuations of the polymer, it is less likely for a polymer to be in a configuration in which an end monomer can thread quickly, in fact, it is substantially more likely that there are many thread attempts before one is favourable enough to permit translocation. Thus, a dominant peak in the distribution emerges, and, as N increases, this effect is heightened in two ways: first, when compared to the standard protocol, compression of the polymer is increased and more likely at higher N (the polymer must wait for an end to thread) which results in a greater number of the short translocation times, and second, as N is increased, there is more variability in the configurations from the capture protocol that successfully thread from elongated states, effectively lengthening the tail of the distribution.

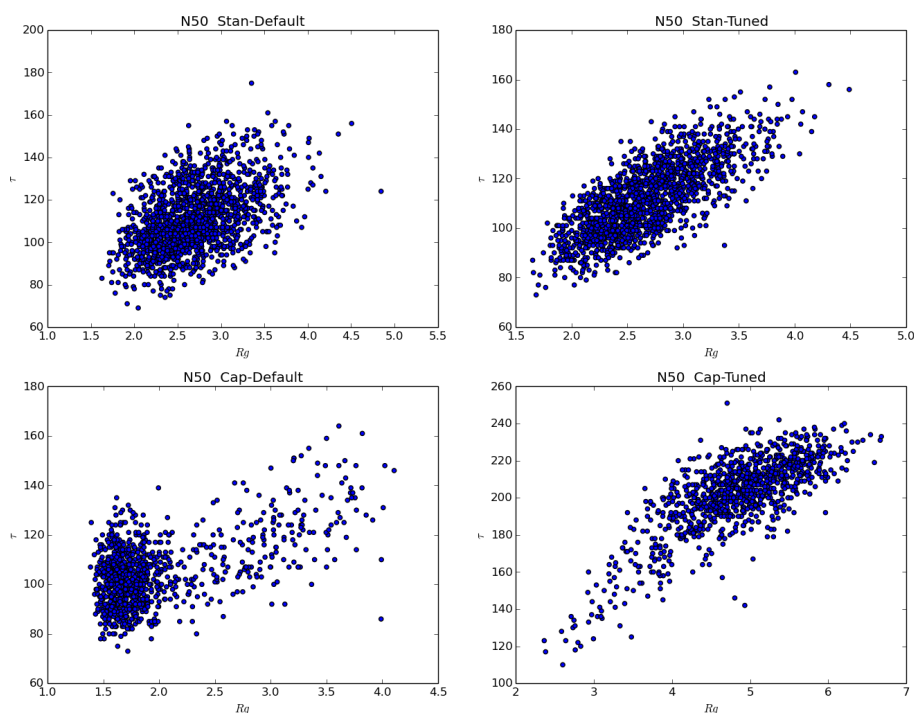


FIGURE 5.11: Scatter plot representing all 2000 successful translocation events for all protocols under both Péclet conditions. Here $N = 50$, R_g is along the x-axis and τ is along the y-axis. Default P is left column, tuned P right column, standard protocol is the top row and capture protocol the bottom row.

Tuned Péclet

Turning to the distribution of τ under tuned Péclet conditions, Fig. 5.10 illustrates the substantial shift in mean translocation time; for all N , τ is found to be considerably longer than any of the other mean translocation times. In contrast to default P conditions, the distribution at tuned P has a slight tail skewed towards shorter τ , but as N is increased, the distribution becomes more symmetric. Unable to fully relax at tuned P , the polymer is always forcibly extended

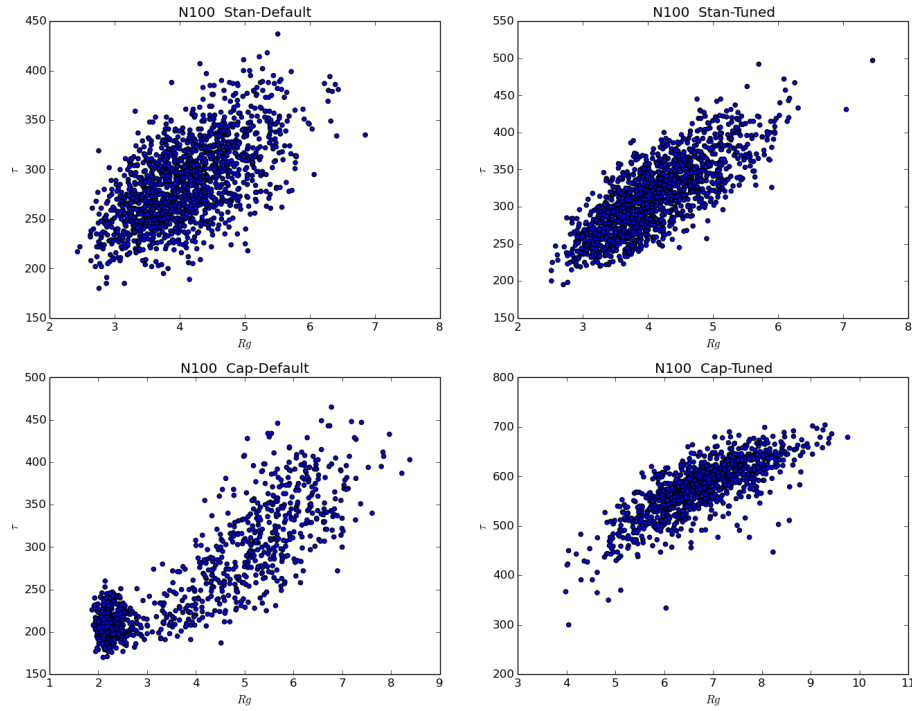


FIGURE 5.12: Scatter plot representing all 2000 successful translocation events for all protocols under both Péclet conditions. Here $N = 100$, R_g is along the x-axis and τ is along the y-axis. Default P is left column, tuned P right column, standard protocol is the top row and capture protocol the bottom row.

and experiences the large drag previously discussed in Sec. 5.3.2. The bottom-right inset of Fig. 5.11-5.13 illustrates how individual translocation events become more evenly spread across R_g and τ values with increasing N .

As N is increased, the number of monomers that are pulled one-by-one into the high-field regions increases the overall drag on the polymer, lengthening τ . At smaller N , there are occasions where the polymer is not caught by an end. If these events lead to successful translocations, they necessarily also lead to longer threading times, compressing the polymer, and as before, result in relatively faster translocation times. These events are those found in the tail to

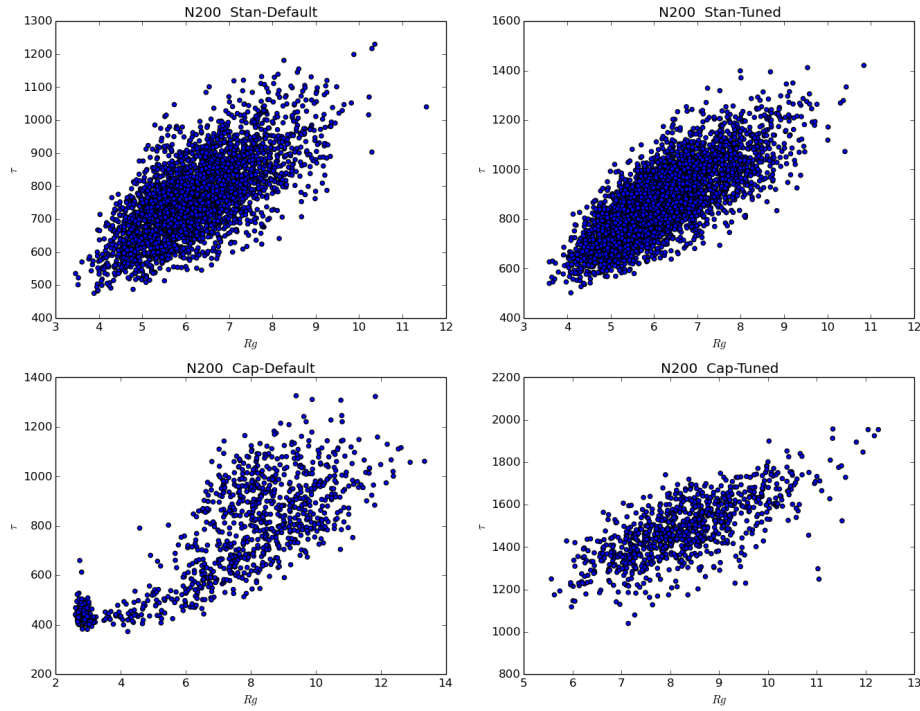


FIGURE 5.13: Scatter plot representing all 2000 successful translocation events for all protocols under both Péclet conditions. Here $N = 200$, R_g is along the x-axis and τ is along the y-axis. Default P is left column, tuned P right column, standard protocol is the top row and capture protocol the bottom row.

short τ of the tuned P distributions of the capture protocol in Fig. 5.10. Corresponding thread times to these short τ are represented by the few thread events occurring at times longer than the main spike in Fig. 5.5.

In contrast, most successful events at tuned P occur with very long translocation times. Fig. 5.5 emphasizes this characteristic where, for all N , nearly all thread times recorded were extremely fast, especially when compared side-by-side to default P conditions. The direct result of arriving extended and on-end to the nanopore is that threading is both quick and likely and there is little

chance of the polymer being compressed against the membrane. In this situation, from contact through to translocation, each monomer must instead pull the monomer directly behind it into the nanopore. As the polymer is increased to even larger N , the translocation time similarly increases as there are more monomers to drag in towards the nanopore. Interestingly, at long enough N , it is possible for a polymer caught in the high field regions to uncurl by an end in such a way that this end, pulling taught a chain of monomers behind it, can reach the mouth of the nanopore while a large portion of the polymer remains (somewhat) coiled still not yet affected by the propagating tension along the chain (recall the tension-propagation front discussed in Ch. 2 and Ch. 3). There is thus a considerable amount of consistent drag on the polymer's movement and this impacts the translocation time- elongated polymers translocate slowly.

5.5 Scaling Results

Fig. 5.14 provides the scaling relationship between translocation time, τ , and polymer length, N , and is typically defined as $\tau \sim N^\alpha$. At this time, most Langevin dynamics simulations of polymer translocation find $\alpha \approx 1.4$ [72, 73]. Note that these simulations are those which employ the standard protocol at Péclet values around default P .

5.5.1 Trends: Standard Protocol

Indeed, simulations performed here under similar conditions find $\alpha = 1.41$ which is consistent with contemporary work in the field. After adjusting to better represent experimental conditions, α increases slightly to 1.43. Although the protocols are the same, Fig. 5.10 shows that at tuned P , mean τ grows slightly

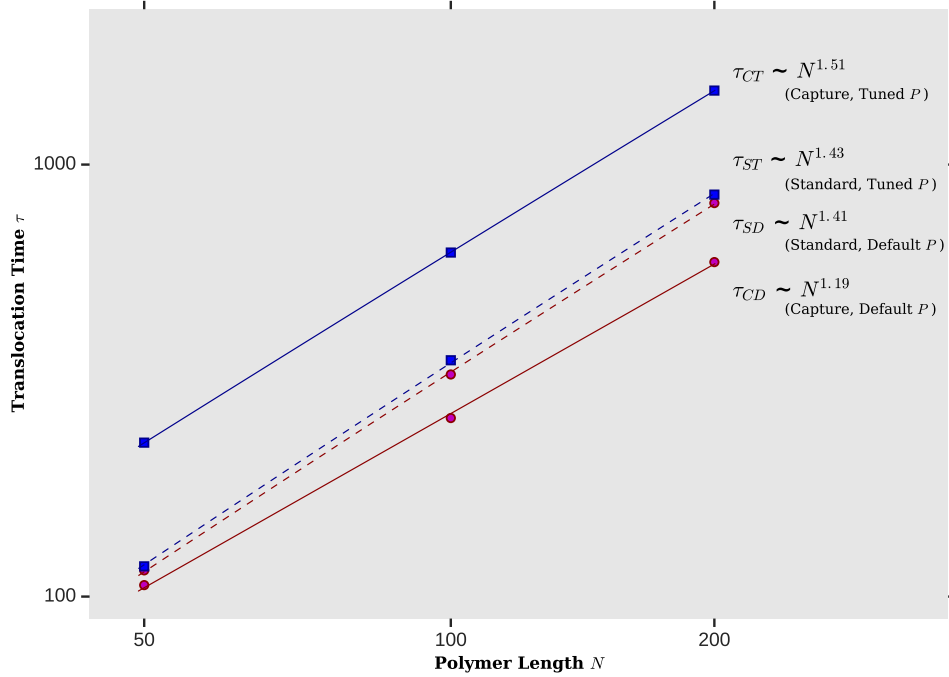


FIGURE 5.14: Scaling results for all conditions. Here, translocation time, τ , is plotted against the polymer length, N . As before, error bars are on the order of the data point. Dashed lines correspond to the standard protocol and are consistent with typical results (scaling exponent $\alpha \simeq 1.4$). By including the capture process in the computational model deviations from typical scaling results are obtained, further illustrating that standard approaches do not necessarily reflect reality.

faster with increasing N . Thus, when diffusion is suppressed, the polymer experiences more drag as N is increased, leading to longer translocation times, and thus a (slightly) larger α .

5.5.2 Trends: Capture Protocol

Returning to Fig. 5.14 it is quite evident that the capture process has a considerable effect on scaling. Since the capture protocol was designed to resemble more

realistic conditions, it appears that simulations run with previous methodologies may, in fact, generate results that are quantitatively incorrect. For the capture protocol with default P , $\alpha = 1.19$ and is considerably lower than either standard protocol result. This lower rate of change reflects the balance that emerges between the time it takes for an end monomer to thread versus the number of monomers total. Without starting prethreaded and able to translocate immediately, as in the standard protocol, the addition of the external field to the capture protocol works to compress the polymer against the membrane. Naturally, the extent of compression will increase as time passes. Since only $2/N$ monomers may thread successfully, there is additional time spent at this phase as N is increased, resulting in increasingly compressed conformations found at default P . As described in Sec. 5.4, compressed states lead to fast translocation times, and indeed, at default P the capture protocol produces some of the fastest translocation times of all.

At the other end of the spectrum, tuned P results have $\alpha = 1.51$. At the low end where $N = 50$, the effect of suppressing diffusion in the capture protocol is already responsible for a considerable increase in τ , as compared to the other simulations, and this effect grows as N is increased. Fig. 5.14 identifies how, for all N , the combination of the capture protocol and tuned P produces longer translocation times. Under these conditions the polymer is unable to relax and is instead forcibly elongated by an end through the effects of the external field. Thus, the polymer (almost) *always* begins a successful translocation event in an extended configuration (recall how polymers unable to thread quickly under tuned P become stuck). The resulting drag on the polymer is additive for each additional monomer that must be pulled in, thereby increasing the rate at which τ changes with longer N .

Chapter 6

CONCLUSION

6.1 Summary

Polymer translocation is a relatively established (small) field, however, due to the inherent complexity involved with biological and nanoscale dynamics, there are plenty of questions still unanswered. The work done here assists in bridging some of these open-ended research pursuits. Current literature is focused on scaling law theories which is often insufficient in describing clear and reliable pictures that are useful to a wider audience. In this work, a simulation methodology of the entire translocation process, including capture, is developed. By monitoring the conformational changes in a polymer as it diffuses towards a nanopore, both the diffusive and drift dynamics of translocation observed may offer some progress in identifying how an initial polymer conformation may affect translocation.

Under standard simulation conditions, the results here are consistent with current literature and produce a scaling exponent of $\alpha \sim 1.4$. When capture is included in the translocation simulations however, a significant departure from the standard α value is obtained. This is consistent with the assumption made that the conformational changes a polymer undergoes prior to translocation

would affect the translocation dynamics. In fact, it was shown that polymer translocation is inherently sensitive to changes in a polymer's configuration prior to translocation and that these changes are linked to the drift-diffusion balance of the system. When diffusion of a system is suppressed, the scaling exponent for translocation was found to increase from the standard value for α . In contrast, simulations of a polymer undergoing the capture process as well as translocation under a drift-diffusion balance typical of standard simulations indicate an α lower than typical values. Here $\alpha = 1.51$ for tuned Péclet and $\alpha = 1.19$ for default Péclet. Although specific values for α are obtained, the emphasis is instead on the relative change in scaling exponent -either increased or decreased- from the accepted standard value for α .

In short, the capture process has a significant and measurable affect on the conformation of a polymer. This in turn affects the nanopore threading dynamics that determine the polymer's rate of translocation. Changes in the Péclet number have a substantial effect on polymer motion and resulting conformations at various stages during the capture-translocation process. Thus, this research emphasizes that the effective simulation of polymer translocation appears to benefit from, and may require, modelling the capture process in addition to including polymer specific characteristics.

6.1.1 Evaluation

TABLE 6.1: Average Durations of Capture Protocol Phases

P value	Polymer Length	Contact	Thread	Translocation
Default Péclet	50	617	750	104
	100	710	1863	230
	200	759	4352	545
Tuned Péclet	50	12667	24	203
	100	16347	32	577
	200	18006	48	1650

Table. 6.1 further emphasizes the differences in duration for the main stages of the capture protocol. Here, the time to contact is included and highlights the computational cost of this important step. Specifically, under tuned Péclet conditions, a considerable amount of time is spent after equilibration waiting for the polymer to diffuse close enough into high-field regions where it may be caught and driven towards the nanopore, resulting in contact. As describe in Sec. 5.3.1 and Sec. 5.3.2, threading (the time from contact through to last thread) is considerably longer at default P , and, for both Péclet numbers, the translocation time increases steadily with N . What is not shown however, is that there are two other possible outcomes during the capture protocol: diffused away and stuck events. Both incur additional computational costs but can be controlled to some extent. After reviewing physical visualizations of the translocation simulations a decision was made to terminate runs under stuck conditions that occurred for $3\tau_{Rx}$ (here τ_{Rx} refers to the relaxation time of the polymer at length, N). The condition for a diffused away event is tied to R_{port} whereby simulations with many diffused away events may benefit from either a) transporting the equilibrated polymer closer to the nanopore at the start or possibly

through b) increasing the cutoff distance for diffused away events. However, if a polymer is released too close to the nanopore the natural conformational changes in the polymer are suppressed as there is insufficient space and time for the polymer to diffuse in towards the nanopore. Thus, the ratio of stuck events to translocation events will likely shift to favour more stuck events, particularly if the time cutoff for a stuck event is a shorter duration (such as the $3\tau_{Rx}$ condition presented here). In this way, it is possible to favour certain outcomes over others as outliers are removed.

The capture protocol was tested under many different conditions; some of which include simulations of additional polymer lengths of $N = 25$ and 300 , transporting the equilibrated polymer to various distances of R_{port} as well as obtaining the shortest time to classify a polymer as 'stuck' and increasing pore sizes to the point of permitting occasional hernias. Additionally, simulations of polymers with varying persistence lengths were initially performed but later abandoned for future work as it soon became clear that a thorough development, analysis and comparison of the capture protocol to standard methodologies was required for even the most general of simulation conditions; the freely-jointed polymer chain and the drift-diffusion balance. The purpose of these conditional tests served to probe the sensitivity of the simulation methodology itself and whether the resulting translocation process results could be altered with seemingly insignificant small changes to the environment. Overall, the capture protocol remained consistent.

The significant deviations from typical scaling results obtained by this work only serve to further illustrate how the capture process is an integral part of the

entire translocation process and should be included in simulation methodologies. Computational cost is nevertheless a notable source of concern in simulation work and the inclusion of the capture process certainly requires careful consideration due to the hefty need for extended computation time. Perhaps, in future work, there may be a way to pre-load specific environmental conditions and polymer conformations that more accurately reflect the drift-diffusion balance and in so doing, bring simulation and experiment into greater agreement.

6.2 The Extended Model

As periodically discussed throughout this work, extensions to the current model have, at present, been successfully adopted. In particular, the E-field used in the model was further refined to incorporate the recent mathematical work by Farahpour et al.[19] and also Kowalczyk et al.[49]. Using an alternative oblate spheroidal coordinate system the changes in the E-field, as constrained by the nanopore geometry, were more clearly defined. The result of including this analysis was an even greater emphasis of the nonequilibrium state of polymer configurations during the capture process- further supporting the work done here. Following the suggestion of a referee, the data from the R_g configuration stages were transformed such that instead of comparing elongation and contraction of the polymer perpendicular and parallel to the nanopore, these conformational changes were compared along an axis parallel to the local E-Field lines. These adjustments were successful in highlighting the dramatic configuration changes that occur during translocation, and, as of Oct. 2016, the results are now published in The Journal of Chemical Physics [92].

6.2.1 Future adaptations

The capture protocol developed here is easily adapted to many other experimental conditions and academic pursuits. The focus on the underlying qualitative picture permits a rich expansion into broad applications. Perhaps most interesting is that a full adaptation of the entire capture process has not yet been adopted into mainstream simulation methodologies. Therefore, there are many possibilities for the future and current polymer translocation work can benefit from the analysis used here. It would certainly be time well spent to take the capture process methodologies employed here and approach several new problems. There are some fascinating dynamics at play with polymers significantly longer than were studied. Similarly, the emergence of theoretical work suggests there may be quantitative reasons for the apparent regime changes in the dynamics experienced on the nanoscale. Thus, simulation methodologies, such as the capture-translocation methodology developed here, provide useful connections between experiment and theory.

Further capture-translocation studies that expand upon the methodology proposed here are encouraged. In particular, analyzing the effect of polymer persistence length on translocation is a natural extension of this work and can be easily implemented. Additionally, this work can be expanded through the inclusion of electrostatic screening and hydrodynamic effects and by modelling the polymer to take on certain characteristics of specific polymers, e.g., the charge effects of dsDNA. Of further interest is the analysis of different pore shapes and sizes, as well as comparing alternative external field profiles.

6.3 Final Remarks

The field of polymer science provides many opportunities for biophysical applications. Integral to many of these processes is the capture of a polymer by a nanopore. Understanding the dynamics of this process can improve current polymer-based technologies as well as provide insight for future applications, and expand upon general biological understanding. The inclusion of the capture process into the simulation methodology used here provides a more realistic interpretation of translocation and identifies the importance of the polymer's nonequilibrium configuration just prior to translocation. Thus, inclusion of the capture process should be emphasized for research that seeks to obtain a more accurate picture of this dynamic process.

Bibliography

- [1] Ramesh Adhikari and Aniket Bhattacharya. “Translocation of a semiflexible polymer through a nanopore in the presence of attractive binding particles”. In: *Phys. Rev. E* 92.3 (Sept. 2015), p. 032711.
- [2] B. Alberts, A. Johnson, J. Lewis, M. Raff, K. Roberts, and P. Walter. *Molecular biology of the cell*. New York, USA: Garland Science, 2008.
- [3] Aksimentiev Aleksij, Heng Jiunn B., Timp Gregory, and Schulten Klaus. “Microscopic Kinetics of DNA Translocation through Synthetic Nanopores”. In: *Biophysical Journal* 87.3 (Sept. 2016). doi: 10.1529/biophysj.104.042960, pp. 2086–2097. ISSN: 0006-3495.
- [4] Hagain Bayley. “Nanopore sequencing: from imagination to reality”. In: *Clinical Chemistry* 61 (2015), pp. 25–31.
- [5] Eric Beamish, Harold Kwok, Vincent Tabard-Cossa, and Michel Godin. “Precise control of the size and noise of solid-state nanopores using high electric fields”. In: *Nanotechnology* 23.40 (2012), p. 405301.
- [6] S Bhakdi and J Trantum-Jensen. “Alpha-toxin of *Staphylococcus aureus*.” In: *Microbiological Reviews* 55.4 (1991), pp. 733–751.
- [7] Somendra M. Bhattacharjee, Achille Giacometti, and Amos Maritan. “Flory theory for Polymers”. In: *arXiv:1308.2414 [cond-mat.stat-mech]* (Nov. 2013).

- [8] A. Bhattacharya, W. H. Morrison, K. Luo, T. Ala-Nissila, S. -C. Ying, A. Milchev, and K. Binder. "Scaling exponents of forced polymer translocation through a nanopore". In: *The European Physical Journal E* 29.4 (2009), pp. 423–429. ISSN: 1292-895X.
- [9] Aniket Bhattacharya. "Translocation Dynamics of a Semiflexible Chain Under a Bias: Comparison with Tension Propagation Theory". In: *Polymer Science* 55.1 (2013), pp. 60–69.
- [10] Kyle Briggs, Martin Charron, Harold Kwok, Timothea Le, Sanmeet Chahal, José Bustamante, Matthew Waugh, and Vincent Tabard-Cossa. "Kinetics of nanopore fabrication during controlled breakdown of dielectric membranes in solution". In: *Nanotechnology* 26.8 (2015), p. 084004.
- [11] Kyle Briggs, Harold Kwok, and Vincent Tabard-Cossa. "Automated Fabrication of 2-nm Solid-State Nanopores for Nucleic Acid Analysis". In: *Small* 10.10 (2014), pp. 2077–2086.
- [12] Spencer Carson and Meni Wanunu. "Challenges in DNA motion control and sequence readout using nanopore devices". In: *Nanotechnology* 26 (2015), p. 074004.
- [13] Ying-Cai Chen, Chao Wang, and Meng-Bo Luo. "Simulation study on the translocation of polymer chains through nanopores". In: *The Journal of Chemical Physics* 127.4 (2007).
- [14] Peng Cheng, Jiajun Gu, Eric Brandin, Kim Young-Rok, Qiao Wang, and Daniel Branton. "Probing single DNA molecule transport using fabricated nanopores". In: *Nano Letters* 4 (2004), pp. 2293–2298.
- [15] Jeffrey Chuang, Yacov Kantor, and Mehran Kardar. "Anomalous dynamics of translocation". In: *Phys. Rev. E* 65 (2001), p. 011802.

- [16] Mingming Ding, Xiaozheng Duan, Yuyuan Lu, and Tongfei Shi. "Flow-Induced Ring Polymer Translocation through Nanopores". In: *Macromolecules* 48.16 (2015), pp. 6002–6007.
- [17] J. L. A. Dubbeldam, A. Milchev, V. G. Rostiashvili, and T. A. Vilgis. "Driven polymer translocation through a nanopore: A manifestation of anomalous diffusion". In: *EPL (Europhysics Letters)* 79.1 (2007), p. 18002.
- [18] J. L. A. Dubbeldam, V. G. Rostiashvili, A. Milchev, and T. A. Vilgis. "Forced translocation of a polymer: Dynamical scaling versus molecular dynamics simulation". In: *Phys. Rev. E* 85.4 (Apr. 2012), p. 041801.
- [19] Farnoush Farahpour, Azadeh Maleknejad, Fathollah Varnik, and Mohammad Reza Ejtehadi. "Chain deformation in translocation phenomena". In: *Soft Matter* 9 (2013), pp. 2750–2759.
- [20] Paul J. Flory. *Principles of Polymer Chemistry*. Cornell University Press, 1953.
- [21] Paul J. Flory. "Spatial Configurations of Macromolecular Chains". Nobel Lecture - Chemistry Laureate. Dec. 1974.
- [22] Paul J. Flory. *Statistical Mechanics of Chain Molecules*. Wiley Online Library, 1969.
- [23] Maria Fyta. "Threading DNA through nanopores for biosensing applications". In: *Journal of Physics: Condensed Matter* 27 (2015), p. 273101.
- [24] Maria Fyta, Simone Melchionna, Massimo Bernaschi, Efthimios Kaxiras, and Sauro Succi. "Numerical simulation of conformational variability in biopolymer translocation through wide nanopores". In: *Journal of Statistical Mechanics: Theory and Experiment* (June 2009).

- [25] Maria Fyta, Simone Melchionna, Sauro Succi, and Efthimios Kaxiras. “Hydrodynamic correlations in the translocation of a biopolymer through a nanopore: Theory and multiscale simulations”. In: *Phys. Rev. E* 78.3 (Sept. 2008), p. 036704.
- [26] M. G. Gauthier and G. W. Slater. “Molecular Dynamics simulation of a polymer chain translocating through a nanoscopic pore”. In: *The European Physical Journal E* 25.1 (2008), pp. 17–23. ISSN: 1292-895X.
- [27] Michel G. Gauthier and Gary W. Slater. “Nondriven polymer translocation through a nanopore: Computational evidence that the escape and relaxation processes are coupled”. In: *Phys. Rev. E* 79.2 (Feb. 2009), p. 021802.
- [28] Pierre-Gilles de Gennes. “Passive Entry of a DNA Molecule into a Small Pore”. In: vol. 96. 13. June 1999, p. 7262.
- [29] Pierre-Gilles de Gennes. *Scaling Concepts in Polymer Physics*. Cornell University Press, 1979.
- [30] Pierre-Gilles de Gennes. “Soft Matter”. Nobel Lecture - Physics Laureate. Dec. 1991.
- [31] G. S. Grest and K. Kremer. “Molecular dynamics simulation for polymers in the presence of a heat bath”. In: *Physical Review, A* 33.3628 (1986).
- [32] Steve Guillouzic and Gary W. Slater. “Polymer translocation in the presence of excluded volume and explicit hydrodynamic interactions”. In: *Physics Letters A* 359.4 (2006), pp. 261–264. ISSN: 0375-9601.
- [33] Jiayi Guo, Xuejin Li, Yuan Liu, and Haojun Liang. “Flow-induced translocation of polymers through a fluidic channel: A dissipative particle dynamics simulation study”. In: *The Journal of Chemical Physics* 134.13 (2011).

- [34] H. W. de Haan, D. Sean, and G. W. Slater. "Using a Peclet number for the translocation of a polymer through a nanopore to tune coarse-grained simulations to experimental conditions". In: *Physical Review, E* 91 (2015), p. 022601.
- [35] H. W. de Haan and T. N. Shendruk. "Force-Extension for DNA in Nanoslit: Mapping between the 3D and 2D limits". In: *ACS Macro Letters* 4 (2015), pp. 632–635.
- [36] H. W. de Haan and Gary W. Slater. "Memory effects during the unbiased translocation of a polymer through a nanopore". In: *The Journal of Chemical Physics* 136.15 (Apr. 2012), p. 154903.
- [37] W. Humphrey, A. Dalke, and K. Schulten. "SHARCNET". In: *Journal of Molecular Graphics* 14 (1996), p. 33.
- [38] William Humphrey, Andrew Dalke, and Klaus Schulten. "VMD – Visual Molecular Dynamics". In: *Journal of Molecular Graphics* 14 (1996), pp. 33–38.
- [39] J. D. Hunter. "VMD". In: *Computing in Science and Engineering* 9 (2007), p. 90.
- [40] Ilkka Huopaniemi, Kaifu Luo, Tapio Ala-Nissila, and See-Chen Ying. "Langevin dynamics simulations of polymer translocation through nanopores". In: *The Journal of Chemical Physics* 125.12 (2006).
- [41] T. Ikonen, A. Bhattacharya, T. Ala-Nissila, and W. Sung. "Influence of non-universal effects on dynamical scaling in driven polymer translocation". In: *The Journal of Chemical Physics* 137.8 (2012).

- [42] T. Ikonen, A. Bhattacharya, T. Ala-Nissila, and W. Sung. "Influence of pore friction on the universal aspects of driven polymer translocation". In: *EPL (Europhysics Letters)* 103.3 (2013), p. 38001.
- [43] T. Ikonen, A. Bhattacharya, T. Ala-Nissila, and W. Sung. "Unifying model of driven polymer translocation". In: *Phys. Rev. E* 85.5 (May 2012), p. 051803.
- [44] Byoung-jin Jeon and Murugappan Muthukumar. "Polymer capture by alpha-hemolysin pore upon salt concentration gradient". In: *The Journal of Chemical Physics* 140 (2014), p. 015101.
- [45] Yacov Kantor and Mehran Kardar. "Anomalous dynamics of forced translocation". In: *Phys. Rev. E* 69 (2004), p. 021806.
- [46] Felix Kapahnke, Ulrich Schmidt, Dieter W. Heermann, and Matthias Weiss. "Polymer translocation through a nanopore: The effect of solvent conditions". In: *The Journal of Chemical Physics* 132.16 (Apr. 2010), p. 164904.
- [47] Stefan Kesselheim, Wojciech Müller, and Christian Holm. "Origin of Current Blockades in Nanopore Translocation Experiments". In: *Phys. Rev. Lett.* 112.1 (Jan. 2014), p. 018101.
- [48] Koehl, Patrick and Levitt, Michael and Edelsbrunner, Herbert. *Implicit Solvent Models for Molecular Simulations*. From ProShape: accessed 2016. URL: <http://csb.stanford.edu/~koehl/ProShape/born.php>.
- [49] Stefan W Kowalczyk, Alexander Y Grosberg, Yitzhak Rabin, and Cees Dekker. "Modeling the conductance and DNA blockade of solid-state nanopores". In: *Nanotechnology* 22.31 (2011), p. 315101.
- [50] H. A. Kramers. "Brownian motion in a field of force and the diffusion model of chemical reactions". In: *Physica* 7 (1940), pp. 284–304.

- [51] Harold Kwok, Kyle Briggs, and Vincent Tabard-Cossa. "Nanopore fabrication by controlled dielectric breakdown". In: *PLoS One* 9.3 (2014), e92880.
- [52] Harold Kwok, Matthew Waugh, José Bustamante, Kyle Briggs, and Vincent Tabard-Cossa. "Long Passage Times of Short ssDNA Molecules through Metallized Nanopores Fabricated by Controlled Breakdown". In: *Advanced Functional Materials* 24.48 (2014), pp. 7745–7753.
- [53] V. V. Lehtola, R. P. Linna, and K. Kaski. "Critical evaluation of the computational methods used in the forced polymer translocation". In: *Phys. Rev. E* 78.6 (Dec. 2008), p. 061803.
- [54] Hui Li, Jing Zhang, Hong Liu, and Chia-chung Sun. "Nondriven Polymer Translocation Through a Nanopore: Scaling for Translocation Time with Chain Length". In: *Chem. Res. Chinese Universities* 27.6 (2011), p. 1023.
- [55] H.-j. Limbach, A. Arnold, B. A. Mann, and C. Holm. "Espresso". In: *Computer Physics Communications* 174 (2016), p. 704.
- [56] K. Luo, T. Ala-Nissila, S.-C. Ying, and R. Metzler. "Driven polymer translocation through nanopores: Slow-vs.-fast dynamics". In: *EPL (Europhysics Letters)* 88.6 (2009), p. 68006.
- [57] Kaifu Luo, T. Ala-Nissila, and See-Chen Ying. "Polymer translocation through a nanopore: A two-dimensional Monte Carlo study". In: *The Journal of Chemical Physics* 124.3 (2006).
- [58] Kaifu Luo, Tapio Ala-Nissila, See-Chen Ying, and Aniket Bhattacharya. "Influence of Polymer-Pore Interactions on Translocation". In: *Phys. Rev. Lett.* 99.14 (Oct. 2007), p. 148102.

- [59] Kaifu Luo, Tapio Ala-Nissila, See-Chen Ying, and Aniket Bhattacharya. "Sequence Dependence of DNA Translocation through a Nanopore". In: *Phys. Rev. Lett.* 100.5 (Feb. 2008), p. 058101.
- [60] Kaifu Luo, Ilkka Huopaniemi, Tapio Ala-Nissila, and See-Chen Ying. "Polymer translocation through a nanopore under an applied external field". In: *The Journal of Chemical Physics* 124.11 (2006).
- [61] Kaifu Luo and Ralf Metzler. "Polymer translocation into a fluidic channel through a nanopore". In: *Phys. Rev. E* 82.2 (Aug. 2010), p. 021922.
- [62] Kaifu Luo and Ralf Metzler. "The chain sucker: Translocation dynamics of a polymer chain into a long narrow channel driven by longitudinal flow". In: *The Journal of Chemical Physics* 134.13 (2011).
- [63] Kaifu Luo, Santtu T. T. Ollila, Ilkka Huopaniemi, Tapio Ala-Nissila, Pawel Pomorski, Mikko Karttunen, See-Chen Ying, and Aniket Bhattacharya. "Dynamical scaling exponents for polymer translocation through a nanopore". In: *Phys. Rev. E* 78.5 (Nov. 2008), p. 050901.
- [64] Silvina Matysiak, Alberto Montesi, Matteo Pasquali, Anatoly B. Kolomeisky, and Cecilia Clementi. "Dynamics of Polymer Translocation through Nanopores: Theory Meets Experiment". In: *Phys. Rev. Lett.* 96.11 (Mar. 2006), p. 118103.
- [65] Angus McMullen, H. W. de Haan, Jay X. Tang, and Derek Stein. "Stiff filamentous virus translocations through solid-state nanopores". In: *Nature Communications* 5 (2014), p. 4171.
- [66] Mirna Mihovilovic, Nicholas Hagerty, and Derek Stein. "Statistics of DNA Capture by a Solid-State Nanopore". In: *Physical Review Letters* 110.2 (2013), p. 028102.

- [67] Andrey Milchev, Kurt Binder, and Aniket Bhattacharya. “Polymer translocation through a nanopore induced by adsorption: Monte Carlo simulation of a coarse-grained model”. In: *The Journal of Chemical Physics* 121.12 (2004), pp. 6042–6051.
- [68] Harri Mökkönen, Timo Ikonen, Tapio Ala-Nissila, and Hannes Jónsson. “Transition state theory approach to polymer escape from a one dimensional potential well”. In: *The Journal of Chemical Physics* 142.22 (2015).
- [69] Muthukumar M. and Kong C. Y. “Simulation of polymer translocation through protein channels”. In: *Proceedings of the National Academy of Sciences* 103.14 (Apr. 2006). 10.1073/pnas.0510725103, pp. 5273–5278.
- [70] Murugappan Muthukumar. *Polymer translocation*. CRC Press, 2011.
- [71] Murugappan Muthukumar. “Polymer translocation through a hole”. In: *The Journal of Chemical Physics* 111 (1999), p. 10371.
- [72] V. V. Palyulin, T. Ala-Nissila, and R. Metzler. “Polymer translocation: the first two decades and recent diversification”. In: *Soft Matter* 10 (2014), pp. 9016–9037.
- [73] Debabrata Panja, Gerard T. Barkema, and Anatoly B. Kolomeisky. “Through the eye of the needle: recent advances in understanding biopolymer translocation”. In: *Journal of Physics: Condensed Matter* 25 (2013), p. 413101.
- [74] James M. Polson. “Polymer translocation into and out of an ellipsoidal cavity”. In: *The Journal of Chemical Physics* 142.17 (2015).
- [75] James M. Polson, Mostafa Fatehi Hassanabad, and Anthony McCaffrey. “Simulation study of the polymer translocation free energy barrier”. In: *The Journal of Chemical Physics* 138.2 (2013).

- [76] Payam Rowghanian and Alexander Y. Grosberg. "Electrophoresis of a DNA coil near a nanopore". In: *Physical Review E* 87 (2013), p. 042723.
- [77] Payam Rowghanian and Alexander Y. Grosberg. "Electrophoretic capture of a DNA chain into a nanopore". In: *Physical Review E* 87 (2013), p. 042722.
- [78] Payam Rowghanian and Alexander Y. Grosberg. "Force-Driven Polymer Translocation through a Nanopore: An Old Problem Revisited". In: *The Journal of Physical Chemistry B* 115.48 (2011), pp. 14127–14135.
- [79] Takuya Saito and Takahiro Sakaue. "Dynamical diagram and scaling in polymer driven translocation". In: *Eur. Phys. J. E* 34 (2012), p. 135.
- [80] Takuya Saito and Takahiro Sakaue. "Process time distribution of driven polymer transport". In: *Physical Review E* 85 (2012), p. 061803.
- [81] Takahiro Sakaue. "Nonequilibrium dynamics of polymer translocation and straightening". In: *Phys. Rev. E* 76.2 (Aug. 2007), p. 021803.
- [82] Takahiro Sakaue. "Sucking genes into pores: Insight into driven translocation". In: *Phys. Rev. E* 81.4 (Apr. 2010), p. 041808.
- [83] Jalal Sarabadani, Timo Ikonen, and Tapio Ala-Nissila. "Iso-flux tension propagation theory of driven polymer translocation: The role of initial configurations". In: *The Journal of Chemical Physics* 141.21 (2014).
- [84] Jalal Sarabadani, Timo Ikonen, and Tapio Ala-Nissila. "Theory of polymer translocation through a flickering nanopore under an alternating driving force". In: *The Journal of Chemical Physics* 143.7 (2015).
- [85] Jay Shendure and Hanlee Ji. "Next-generation DNA sequencing". In: *Nature Biotechnology* 26 (2008), pp. 1135–1145.

- [86] Gary W. Slater, Christian Holm, Mykyta V. Chubynsky, Hendrick W. de Haan, Antoine Dubé, Kai Grass, Owen A. Hickey, Christine Kingsbury, David Sean, Tyler N. Shendruk, and Lixin Zhan. “Modeling the separation of macromolecules: A review of current computer simulation methods”. In: *Electrophoresis* 30 (2009), pp. 792–818.
- [87] Arnold J. Storm, Cornelis Storm, Jianghua Chen, Henny Zandbergen, Jean-Francois Joanny, and Cees Dekker. “Fast DNA translocation through a solid-state nanopore”. In: *Nano Letters* 5 (2005), pp. 1193–1197.
- [88] P. M. Suhonen and R. P. Linna. “Chaperone-assisted translocation of flexible polymers in three dimensions”. In: *Phys. Rev. E* 93.1 (Jan. 2016), p. 012406.
- [89] W. Sung and P. J. Park. “Polymer translocation through a pore in a membrane”. In: *Physical Review Letters* 77 (1996), p. 783.
- [90] Pu Tian and Grant D. Smith. “Translocation of a polymer chain across a nanopore: A Brownian dynamics simulation study”. In: *The Journal of Chemical Physics* 119.21 (2003), pp. 11475–11483.
- [91] Sarah Vollmer. “translocation: a nonequilibrium process”. Poster presented at the Chemical BioPhysics Symposium, Toronto, ON. Apr. 2015.
- [92] Sarah C. Vollmer and Hendrick W. de Haan. “Translocation is a Nonequilibrium Process at All Stages: Simulating the Capture and Translocation of a Polymer by a Nanopore”. In: *The Journal of Chemical Physics* 145.15 (2016).
- [93] Wanunu Meni, Morrison Will, Rabin Yitzhak, Grosberg Alexander Y., and Meller Amit. “Electrostatic focusing of unlabelled DNA into nanoscale pores using a salt gradient”. In: *Nat Nano* 5.2 (Feb. 2010), pp. 160–165. ISSN: 1748-3387.

-
- [94] John D. Weeks, David Chandler, and Hans C. Andersen. “Role of Repulsive Forces in Determining the Equilibrium Structure of Simple Liquids”. In: *The Journal of Chemical Physics* 54.12 (1971), pp. 5237–5247.
- [95] Dongshan Wei, Wen Yang, Xigao Jin, and Qi Liao. “Unforced translocation of a polymer chain through a nanopore: The solvent effect”. In: *The Journal of Chemical Physics* 126.20 (2007).
- [96] Eric W. Weisstein. *Oblate Spheroidal Coordinates*. From MathWorld—A Wolfram Web Resource: accessed 2016. URL: <http://mathworld.wolfram.com/OblateSpheroidalCoordinates.html>.